iScience

CellPress
OPEN ACCESS

Article

Myofiber androgen receptor increases muscle strength mediated by a skeletal muscle splicing variant of Mylk4

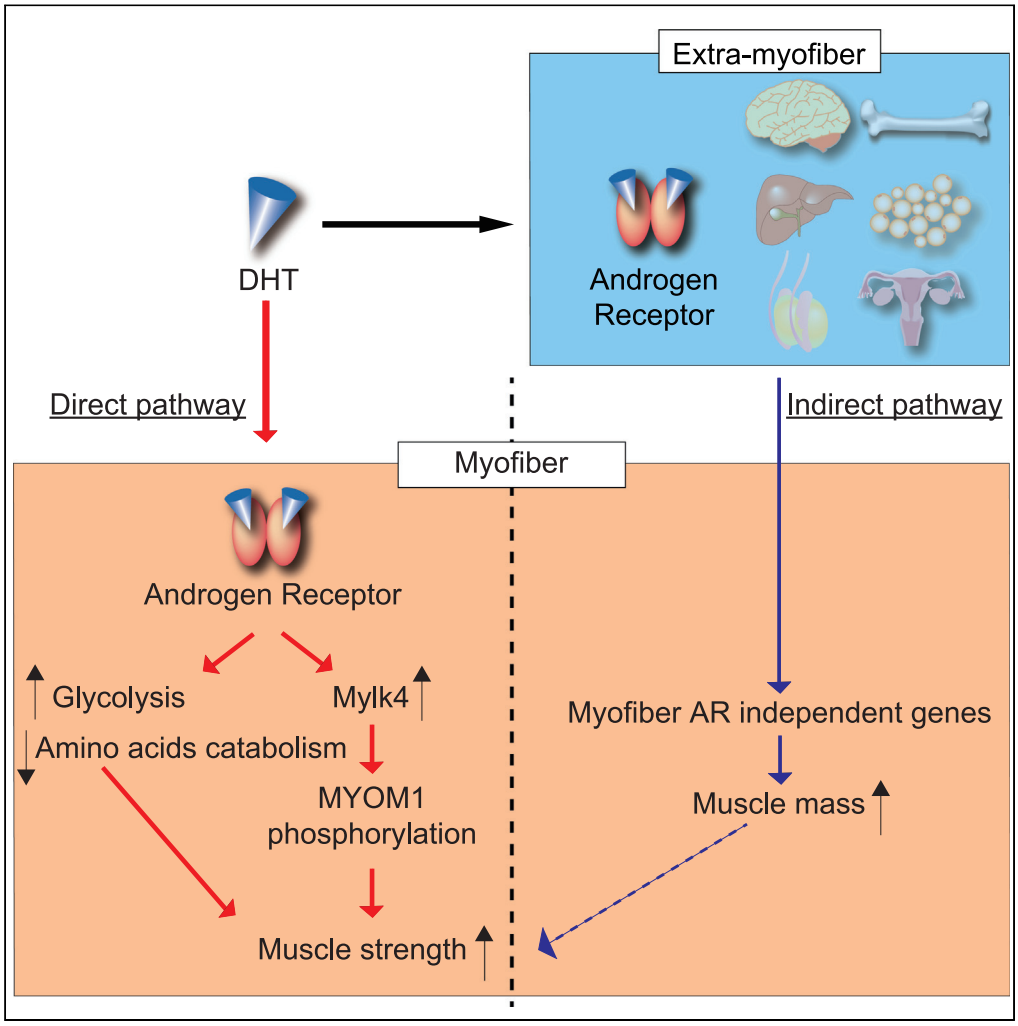

Iori Sakakibara, Yuta Yanagihara, Koichi Himori, ..., So-ichiro Fukada, Tatsuya Sawasaki, Yuuki Imai

y-imai@m.ehime-u.ac.jp

Highlights

DHT increases muscle strength through myofiber AR

Myofiber AR increases a fast-type muscle-specific novel splicing variant of *Mylk4*

MYLK4 regulates muscle strength and muscle stiffness

MYLK4 induces phosphorylation of MYOM1

Sakakibara et al., iScience *24*, 102303
April 23, 2021
https://doi.org/10.1016/j.isci.2021.102303

iScience

CellPress
OPEN ACCESS

Article

Myofiber androgen receptor increases muscle strength mediated by a skeletal muscle splicing variant of Mylk4

Iori Sakakibara,[1,2,3] Yuta Yanagihara,[1,4] Koichi Himori,[5] Takashi Yamada,[5] Hiroshi Sakai,[1,2] Yuichiro Sawada,[1,6] Hirotaka Takahashi,[7] Noritaka Saeki,[1,4] Hiroyuki Hirakawa,[8] Atsushi Yokoyama,[9] So-ichiro Fukada,[10] Tatsuya Sawasaki,[7] and Yuuki Imai[1,2,4,11,12,*]

SUMMARY

Androgens have a robust effect on skeletal muscles to increase muscle mass and strength. The molecular mechanism of androgen/androgen receptor (AR) action on muscle strength is still not well known, especially for the regulation of sarcomeric genes. In this study, we generated androgen-induced hypertrophic model mice, myofiber-specific androgen receptor knockout (cARKO) mice supplemented with dihydrotestosterone (DHT). DHT treatment increased grip strength in control mice but not in cARKO mice. Transcriptome analysis by RNA-seq, using skeletal muscles obtained from control and cARKO mice treated with or without DHT, identified a fast-type muscle-specific novel splicing variant of *Myosin light-chain kinase 4 (Mylk4)* as a target of AR in skeletal muscles. *Mylk4* knockout mice exhibited decreased maximum isometric torque of plantar flexion and passive stiffness of myofibers due to reduced phosphorylation of Myomesin 1 protein. This study suggests that androgen-induced skeletal muscle strength is mediated with Mylk4 and Myomesin 1 axis.

INTRODUCTION

Androgens are steroid hormones, which are ligands of the androgen receptor (AR) (Chang et al., 2013). Testosterone is produced mainly in the testis and has weak ligand activity against AR. 5α-reductase converts testosterone to 5α-dihydrotestosterone (5α-DHT), which is a more potent metabolite to AR compared with testosterone (Burd et al., 2006). While DHT is more potent, it is synthesized almost exclusively in the skin, liver, and gonads such that the major circulating androgen is testosterone. Androgen binding to AR leads to nuclear translocation of AR, and a ligand-bound AR protein forms a complex with transcriptional coregulators to regulate target gene transcription. AR is expressed in various tissues to achieve specific physiological functions. One target of androgens is skeletal muscle, and supraphysiological doses of androgens increase muscle mass and strength (Basaria et al., 2010; Bhasin et al., 2001).

Skeletal muscle contraction is achieved by concerted action of sarcomeric proteins. During a resting state, a troponin complex, consisting of troponin T, troponin C (TNNC), and troponin I, inhibits myosin heavy chain (MyHC) ATPase activity. Motoneuron firing stimulates intramyofibrillar Ca^{2+} release from sarcoplasmic reticulum, and Ca^{2+} binds to TNNC, which induces conformational change and enables MyHC ATPase to act as a motor protein (Schiaffino and Reggiani, 2011). Four isoforms of MyHC proteins (MyHCI, MyHCIIA, MyHCIIX, and MyHCIIB) are present in the adult mouse limb. These MyHC proteins potentiate different ATPase activity, which results in different muscle contraction force. MyHC proteins are bound by two essential myosin light chains (MyLCs), essential MyLC and regulatory MyLC, which play a modulatory role in maximum shortening velocity. Cytosolic Ca^{2+} also forms a complex with calmodulin, and a Ca^{2+}/calmodulin complex further binds to myosin light-chain kinase 2 (MLCK2), which phosphorylates regulatory MyLC to increase frequency-dependent potentiation of skeletal muscle contraction (Stull et al., 2011; Zhi et al., 2005). Thus, skeletal muscle strength is regulated by the amounts or functional status of sarcomeric proteins.

Dozens of studies about androgen action on skeletal muscles have been reported (De Gendt and Verhoeven, 2012). Global AR-deficient male mice exhibited low muscle mass and low muscle contraction force in

[1]Division of Integrative Pathophysiology, Proteo-Science Center, Ehime University, Shitsukawa, Toon, Ehime 791-0295, Japan

[2]Department of Pathophysiology, Ehime University Graduate School of Medicine, Toon, Ehime 791-0295, Japan

[3]Department of Nutritional Physiology, Institute of Medical Nutrition, Tokushima University Graduate School, Tokushima 770-8503, Japan

[4]Division of Laboratory Animal Research, Advanced Research Support Center, Ehime University, Toon, Ehime 791-0295, Japan

[5]Graduate School of Health Sciences, Sapporo Medical University, Sapporo, Hokkaido 060-8558, Japan

[6]Department of Urology, Ehime University Graduate School of Medicine, Toon, Ehime 791-0295, Japan

[7]Division of Cell-Free Sciences, Proteo-Science Center (PROS), Ehime University, Matsuyama, Ehime 790-8577, Japan

[8]Department of Physiology and Cell Biology, Tokyo Medical and Dental University (TMDU), Graduate School, Tokyo 113-8510, Japan

[9]Department of Molecular Endocrinology, Tohoku University Graduate School of Medicine, Sendai, Miyagi 980-8575, Japan

[10]Project for Muscle Stem Cell Biology, Graduate School of Pharmaceutical Sciences, Osaka University, Suita, Osaka 565-0871, Japan

[11]Research Unit for Skeletal Health and Diseases, Ehime University, Toon, Ehime 791-0295, Japan

Continued

hindlimb muscles, which indicated that AR is essential for muscle mass and strength in male mice (MacLean et al., 2008; Ophoff et al., 2009). Several lines of skeletal muscle-specific AR knockout (ARKO) mice have been generated by crossing three lines of AR floxed mice (Ar^{tm2Ska}, $Ar^{tm1Verh}$, or Ar^{tm1Jdz}) and transgenic mice expressing Cre recombinase under the control of the human skeletal actin promoter (HSA-Cre, myocytes), muscle creatine kinase (MCK-Cre, myocytes), or Myod promoter (Myod-iCre, myogenic progenitor cells) (De Gendt and Verhoeven, 2012). Almost all the skeletal muscle-specific ARKO mice showed reduced LA (levator ani) muscle mass and muscle grip strength or tibialis anterior (TA) muscle contraction force but did not show reduction of limb muscle mass (Chambon et al., 2010; Dubois et al., 2014; Ferry et al., 2014; Fraysse et al., 2014; Ophoff et al., 2009; Rana et al., 2016). These results of various muscle-specific ARKO mice showed that although LA muscle mass and limb muscle strength is regulated by myofiber AR, most limb muscle mass (gastrocnemius, TA, extensor digitorum longus, soleus muscle) is not regulated by myofiber AR. Some studies reported that myofiber AR could have a role in mitochondrial maintenance, but a molecular mechanism of AR action on muscle strength in limb muscles still remains elusive, especially for the regulation of sarcomeric genes.

In this paper, we established muscle-specific AR knockout mice and a fast-type muscle hypertrophic model using DHT pellet implantation. RNA sequencing provided a key to understand the molecular mechanism of AR function in fast-type skeletal muscle. We propose a new model of androgen/AR actions on fast-type skeletal muscle strength.

RESULTS

AR deficiency in myofiber impairs muscle strength

To characterize the role of AR in adult skeletal muscles, we generated myofiber-specific AR knockout (*cARKO*) mice and implanted a biodegradable pellet containing 10 mg DHT in 9-week-old female mice to avoid the effects of endogenous androgens. One month after implantation, grip strength and muscle weight were measured (Figure 1A). Serum DHT levels were significantly increased by 20 fold in mice supplemented with DHT (Figure 1B). Deletion of AR mRNA was confirmed by quantitaive reverse transcription PCR (RT-qPCR) (Figure 1C). Nuclear AR signals were observed in TA muscles of Ctrl mice supplemented with DHT, which is strongly decreased in TA muscles of *cARKO* mice supplemented with DHT (Figure 1D). Consistent with previous reports (Chambon et al., 2010; Ferry et al., 2014; Fraysse et al., 2014), Ctrl mice increased grip strength by implantation of a DHT pellet, but grip strength in *cARKO* mice did not increase (Figure 1E). Body weight and skeletal muscle weight were increased by DHT treatment at a similar level even in *cARKO* mice (Figures 1F and 1G). These results are consistent with previous reports (Chambon et al., 2010; Ferry et al., 2014; Fraysse et al., 2014) and suggested that grip strength is regulated by myofiber AR and DHT, and muscle mass is regulated by DHT but not through myofiber AR.

To clarify the responsible cell type for androgen-dependent muscle mass regulation, we generated $Pax7^{CreERT2+}$; AR^{flox} mice (*satARKO*) and implanted a pellet containing 10 mg DHT in 9-week-old female mice, as in *cARKO* mice. TA, quadriceps, and gastrocnemius muscle mass increased in *satARKO* mice (Figure S1). This result indicated that AR in satellite cells is not important for the regulation of muscle mass under the conditions of the experiment.

RNA-seq analysis revealed direct targets of AR in skeletal muscle

To clarify the mechanism of DHT- and AR-dependent enhancement of muscle strength, AR target genes in skeletal muscles were analyzed by RNA-seq in the gastrocnemius muscles of Ctrl and *cARKO* mice implanted with a DHT pellet (Figure 2A). As a result, 529 genes were identified as differentially expressed genes (DEGs) with statistical significance ($q < 0.05$) and were classified by their expression patterns into two major groups: myofiber AR- and DHT-dependent genes and myofiber AR-independent DHT-dependent genes (Figure 2B). Considering the phenotypes of *cARKO* mice, myofiber AR- and DHT-dependent genes regulate muscle strength and myofiber AR-independent DHT-dependent genes regulate muscle mass. To analyze the direct effects of AR in a skeletal muscle, Kyoto Encyclopedia of Genes and Genomes (KEGG) pathway analyses were performed with AR- and DHT-dependent upregulated or downregulated genes (Figures 2C and 2D). Sucrose metabolism was identified as an upregulated pathway, and amino acid catabolism and cardiac muscle contraction were identified as downregulated pathways. These results suggested that glucose/amino acid metabolism and/or muscle sarcomeric gene regulation is a key factor for muscle strength.

[12]Lead contact

*Correspondence:
y-imai@m.ehime-u.ac.jp

https://doi.org/10.1016/j.isci.2021.102303

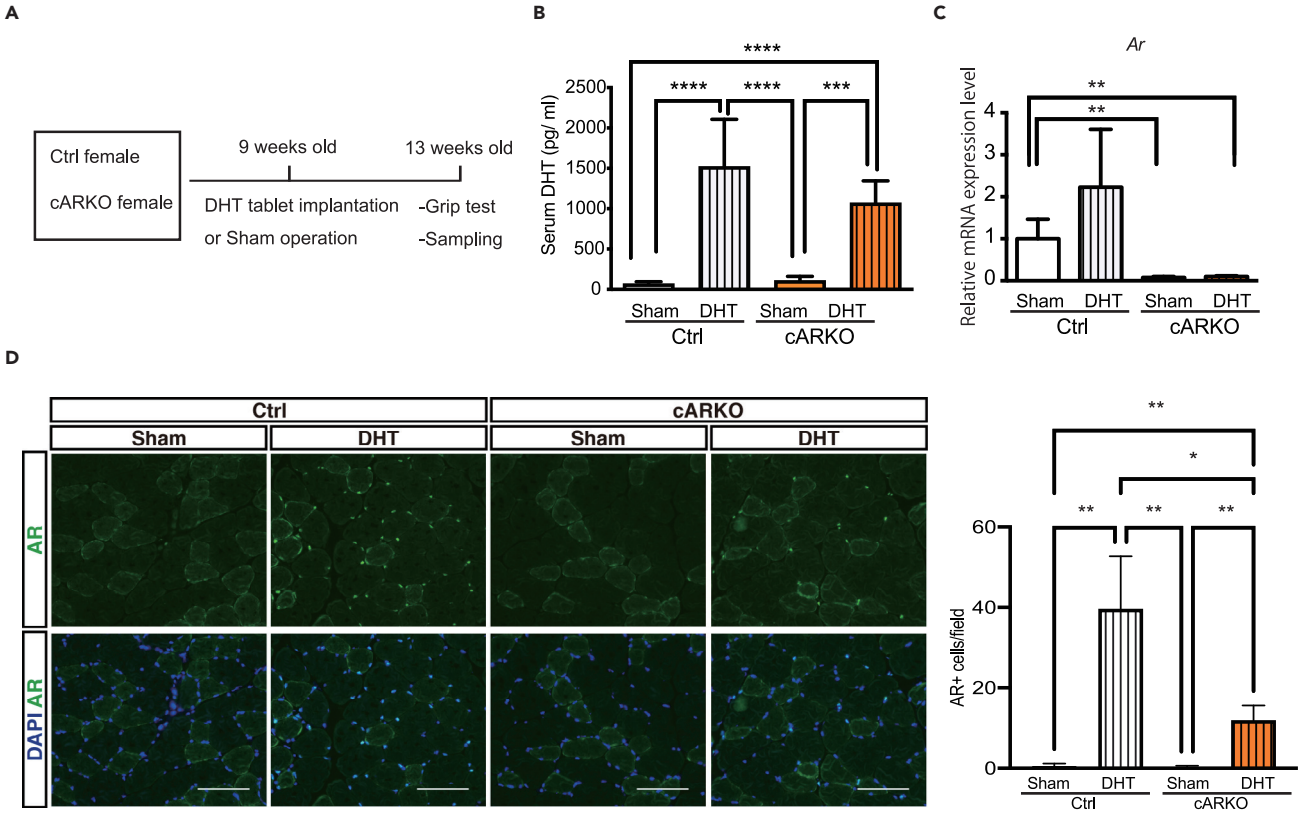
A
Ctrl female
cARKO female
9 weeks old
13 weeks old
DHT tablet implantation
or Sham operation
-Grip test
-Sampling
B
Serum DHT (pg/ ml)
Sham DHT Sham DHT
Ctrl cARKO
C
Ar
Relative mRNA expression level
Sham DHT Sham DHT
Ctrl cARKO
D
Ctrl
cARKO
Sham
DHT
AR
DAPI AR
AR+ cells/field
Sham DHT Sham DHT
Ctrl cARKO
E
Grip strength
Force (N)
Sham DHT Sham DHT
Ctrl cARKO
F
Body Weight
Weight (g)
Sham DHT Sham DHT
Ctrl cARKO
G
TA
Weight (mg)
Sham DHT Sham DHT
Ctrl cARKO
H
Quadriceps
Weight (mg)
Sham DHT Sham DHT
Ctrl cARKO
I
Gas
Weight (mg)
Sham DHT Sham DHT
Ctrl cARKO

Figure 1. *cARKO* female mice showed impaired muscle strength induced by DHT treatment

(A) Experimental scheme. Nine-week-old female control and *cARKO* mice were implanted with a pellet containing 10 mg DHT. Grip strength and tissue weight were measured at 13 weeks old.

(B) Serum DHT levels were determined in 13-week-old female Control_Sham (n = 8), Control_DHT (n = 7), cARKO_Sham (n = 5), and cARKO_DHT (n = 6) mice.

(C) *Ar* mRNA expression levels in gastrocnemius muscles of 13-week-old female Control_Sham (n = 4), Control_DHT (n = 3), cARKO_Sham (n = 4), and cARKO_DHT (n = 5) mice.

(D) Immunostaining of AR in TA muscles. Scale bars: 100 μm.

(E) Grip strength were measured in 13-week-old female Control_Sham (n = 9), Control_DHT (n = 7), cARKO_Sham (n = 9), and cARKO_DHT (n = 7) mice.

(F–I) body weight (F), TA muscle weight (G), quadriceps muscle weight (H), and gastrocnemius muscle weight (I) were measured in 13-week-old female Control_Sham (n = 8), Control_DHT (n = 7), cARKO_Sham (n = 5), and cARKO_DHT (n = 6) mice. Data are represented as mean ± standard deviation. *P < 0.05, **P < 0.01, ***P < 0.001. One-way analysis of variance followed by Student Newman-Keuls tests.

See also Figure S1.

To understand the metabolic change, we visualized DEGs as a metabolic map (Figure S2A). This map clearly indicates that AR increased the gene expression for glycolysis through *Slc2a3*, *Hk2*, and *Agl* and for amino acid import through *Slc38a2*, *Sla38a4*, and *Slc15a5*, but the genes for branched chain amino acid degradation (*Bckdha*, *Dbt*, and *Ivd*) were decreased. Notably, polyamine synthesis-related genes (*Odc1*, *Amd1*, *Mtr*, and *Smox*) were highly upregulated by AR, which is consistent with previous reports (Lee and MacLean, 2011), and this was confirmed by RT-qPCR (Figure S2B). To validate gene expression in wild-type male and female mice, the expression levels of *Odc1*, *Amd1*, and *Smox* were higher in fast-twitch skeletal muscles of male mice compared with those of female mice, although there was no difference in slow-twitch skeletal muscles (Figure S2C). These results suggested that metabolic changes associated with AR prevent amino acid catabolism and provide amino acids for protein production.

Mylk4 was induced by muscle AR

Androgen-induced metabolic changes especially for polyamine synthesis in muscle have been already reported (Lee and MacLean, 2011). In addition to the metabolic pathways, pathways related with sarcomeres were also identified from KEGG pathway analysis. Muscle sarcomere structure is critical to achieve muscle contraction, so the DEGs related to muscle sarcomere structure were visualized in a sarcomere model (Figure 3A). *Mylk4*, *Myh1*, *Musk*, and *Myoz1* were upregulated, and *Actc1*, *Mybph*, *Cacna1s* were downregulated by DHT and AR. Given that the muscle strength in control mice treated with DHT was increased, we focused on the upregulated genes. Among these genes, the upregulation of *Mylk4* and *Myh1* was confirmed by RT-qPCR in an AR- and DHT-dependent manner (Figure 3B). Among them, we hypothesized that *Mylk4* is a possible candidate responsible for increased muscle strength because *Mylk2* is known as a positive regulator of muscle strength (Stull et al., 2011; Zhi et al., 2005). There are four *Mylk* genes in the mouse genome (*Mylk1-4*), and the expression levels of *Mylk* genes were shown from RNA-seq analysis (Figure 3C). Both *Mylk2* and *Mylk4* were expressed in skeletal muscles at similar fragments per kilobase of exon per million mapped reads values, but only *Mylk4* was regulated by AR and DHT. Several splicing variants of *Mylk4* have been found, and a cardiac splicing variant of *Mylk4* has been reported (Chang et al., 2016). To identify splicing variants expressed in skeletal muscles, the *Mylk4* sequence read by RNA-seq was visualized by a genome browser and matched to the *Mylk4* splicing variant (XM_006516667.2, *skmMylk4*), which is different from the cardiac splicing variant of *Mylk4* (Figure 3D). Recently, the existence of the same *Mylk*4 splicing variant (XM_006516667.2) also was reported by an RNA-seq analysis of various skeletal muscles (Terry et al., 2018). The expression of the *Mylk4* splicing variant (XM_006516667.2) was confirmed by real-time PCR with specific primers for the *Mylk4* splicing variant (XM_006516667.2) (Figure 3E). We also examined *Mylk4* expression in male and female tissues (Figure 3F). *Mylk4* is mainly expressed in fast-twitch skeletal muscles (TA, Gas, and quadriceps muscles) and not in hearts or slow-twitch muscles (soleus muscles), and the expression levels of *Mylk4* in male mice are higher than those in female mice. In addition, AR-binding capacity to the promotor region of the *Mylk4* gene was confirmed by registered genome-wide chromatin immunoprecipitaton sequencing data against AR in mouse prostates (Figure S4), suggesting that Mylk4, especially the skeletal muscle splicing variant, could be a direct target of myofiber AR in skeletal muscles.

Decreased isometric torque and impaired passive stiffness in *Mylk4* knockout mice

To clarify the *Mylk4* role in muscle strength, we generated *Mylk4* knockout (KO) mice by a CRISPR/CAS9 system. The guide RNAs were designed at exon 2 and exon 3 of the *Mylk4* gene (Figure 4A), and deletion of the *Mylk4* genome DNA sequence was confirmed by sequencing (Figure 4B). *Mylk4* KO mice were viable and born at the expected Mendelian ratio. The body weight of *Mylk4* KO mice was slightly decreased (Figure 4C), while muscle weight of the gastrocnemius muscle was not different (Figure 4D). However, maximum isometric torque normalized by the whole weight of the PF muscles of *Mylk4* KO mice was

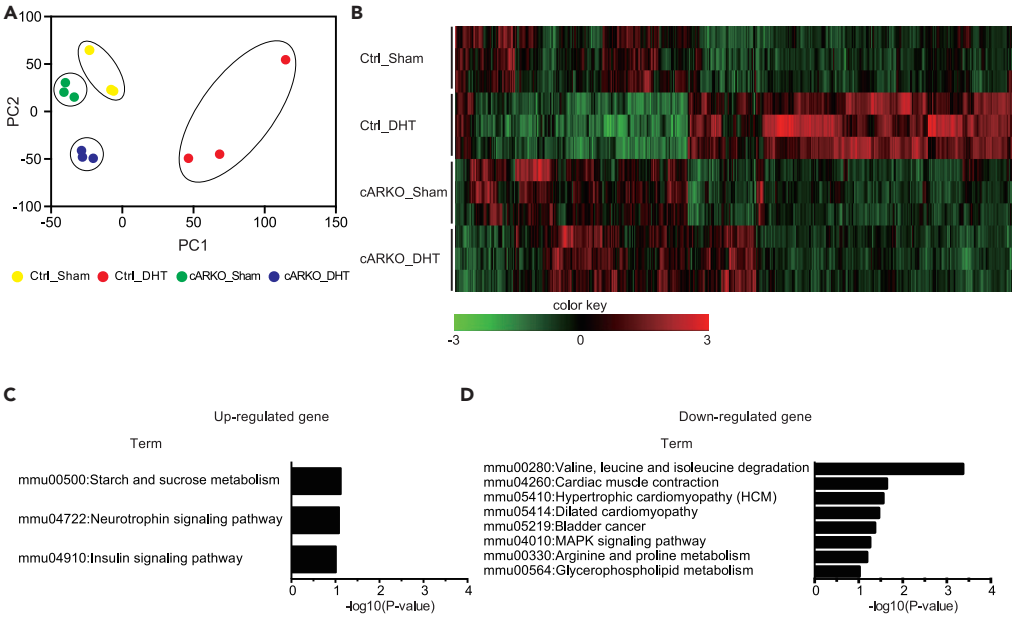

Figure 2. RNA-seq analysis revealed AR- and DHT-dependent transcription

(A and B) (A) Principal components analysis with RNA-seq analysis of gastrocnemius muscles of 13-week-old female Control_Sham, Control_DHT, cARKO_Sham, and cARKO_DHT mice (n = 3, each group) (B) Hierarchical clustering of 529 DEGs in RNA-seq analysis of gastrocnemius muscles of 13-week-old female Control_Sham, Control_DHT, cARKO_Sham, and cARKO_DHT mice (n = 3, each group).

(C and D) KEGG pathway analysis for AR- and DHT-dependent upregulated genes (C) and downregulated genes (D). See also Figures S2 and S3.

significantly decreased compared with wild-type littermate control mice (Figure 4E). These results supported the hypothesis that *Mylk4* contributes to AR-induced muscle strength increase.

As *Mylk2* is known to regulate post-tetanic potentiation (Stull et al., 2011; Zhi et al., 2005), we first hypothesized that *Mylk4* KO mice showed reduced muscle strength through post-tetanic potentiation-dependent manner. However, to our surprise, post-tetanic potentiation was not changed in *Mylk4* KO mice (Figure 4F). Also, the amino acid sequence of Mylk4 is largely distinguished from Mylk2 except for the kinase domain (Figure S5). These results suggested that *Mylk4* has a distinct role compared with *Mylk2*. Next, we focused on substrate preference of a skeletal muscle splicing variant of Mylk4. A cardiac splicing variant of *Mylk4* has been reported to have kinase activity against a regulatory MyLC (Chang et al., 2016). Meanwhile, the N terminal amino acid sequence is completely different between a cardiac splicing variant and a skeletal muscle splicing variant of Mylk4 (Figure S5), which might affect substrate preference of a skeletal muscle splicing variant of Mylk4. To identify substrates of Mylk4 in skeletal muscles, we performed phospho-proteomics analysis with TA muscles from *Mylk4* KO mice (Figure 4G). Phosphorylated proteins were enriched from the lysates of the TA muscles and analyzed by sodium dodecyl sulfate polyacrylamide gel electrophoresis (SDS-PAGE) and Coomassie brilliant blue (CBB) staining, and we found that the signal of one band at around 200 kDa was apparently decreased in *Mylk4* KO mice (Figure 4H). Mass spectrometry analysis identified the band as MYOM1 (Myomesin 1) protein, which is a structural protein of the sarcomeric M band (Obermann et al., 1997). MYOM1 protein level in skeletal muscle was comparable between wild type and *Mylk4 KO* mice (Figure S6), suggesting that Mylk4 affects phosphorylation but not protein level of MYOM1. To confirm this result, we introduced the *in vivo* siRNA against *Mylk4* into TA muscles (Figure S7A). The efficiency of *Mylk4* knockdown was confirmed by RT-qPCR (Figure S7B). Phosphorylated proteins were enriched from the lysates of the TA muscles and SDS-PAGE followed by CBB staining showed the same as for *Mylk4* KO mice (Figure S7C). As a result, a decreased protein level of phosphorylated MYOM1 protein also was confirmed by *in vivo* siRNA for Mylk4. Next, to examine the stiffness of sarcomeric structure because MYOM1 is a component of the sarcomeric M band, we performed skinned fiber analysis with TA muscles from *Mylk4* KO mice and WT littermates. Active force was not changed but passive stiffness was significantly decreased in *Mylk4* KO mice (Figure 4I), suggesting deteriorating function of MYOM1.

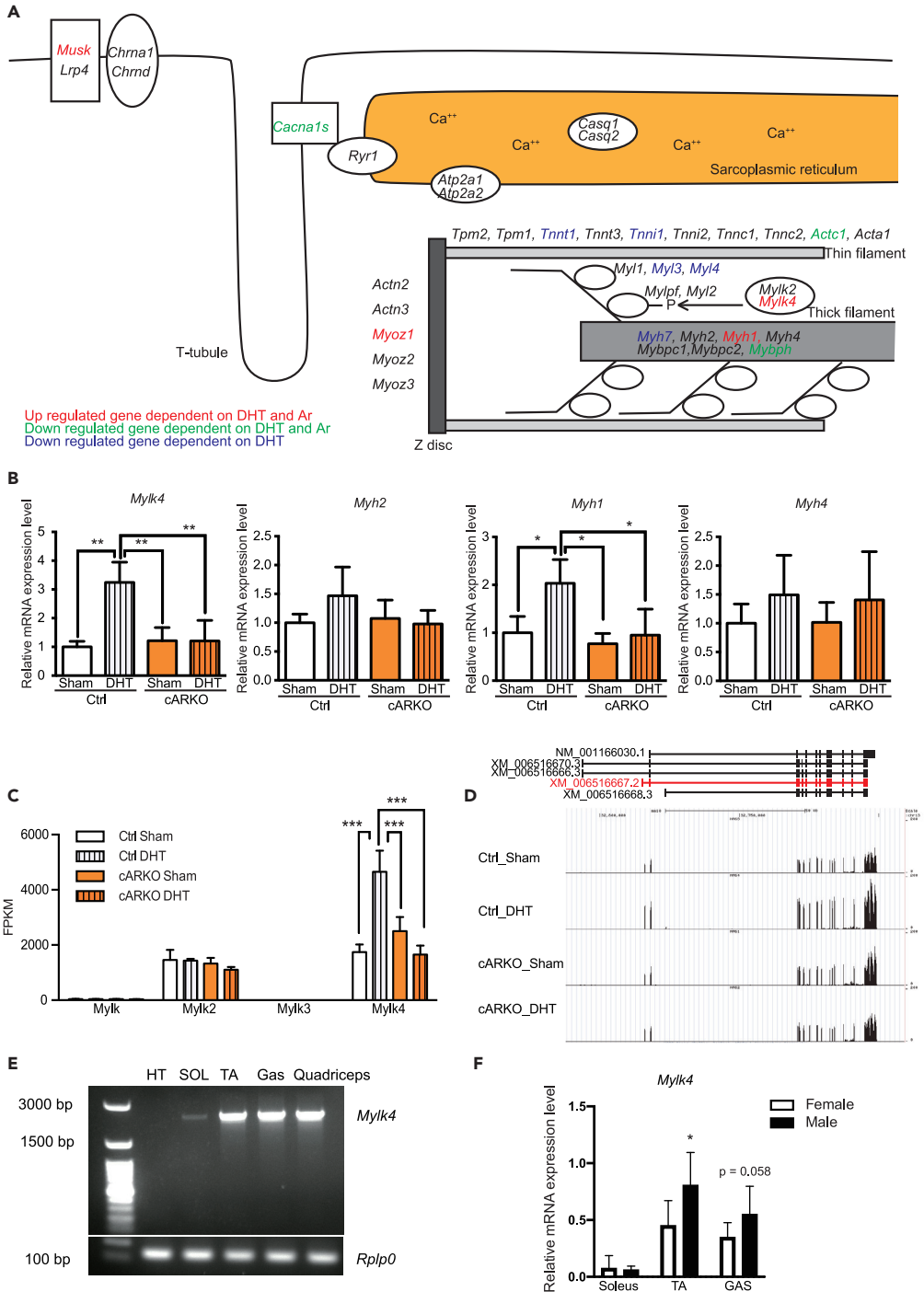

Figure 3. AR induced skeletal muscle-specific splicing variant of *Mylk4* gene expression

(A) A muscle sarcomere model showing AR- and DHT-dependent upregulated or downregulated genes.

(B) mRNA expression levels of *Mylk4, Myh2, Myh1, and Myh4* in gastrocnemius muscles of 13-week-old female Control_Sham (n = 4), Control_DHT (n = 3), cARKO_Sham (n = 4), and cARKO_DHT (n = 5) mice. *P < 0.05, **P < 0.01, ***P < 0.001.

(C) FPKM (fragments per kilobase of exon per million reads mapped) values of *Mylk* genes.

(D) Schematic image of Mylk4 gene locus.

(E) Real-time-PCR analysis of skeletal muscle-specific splicing variants of *Mylk4*.

Figure 3. *Continued*
(F) *Mylk4* gene expression was determined in soleus muscles, TA muscles, and gastrocnemius muscles of male or female mice by RT-qPCR (n = 8, each tissue). Data are represented as mean ± standard deviation. *P < 0.05. One-way analysis of variance followed by Student Newman-Keuls tests.
See also Figures S4 and S5.

These results indicate that the skeletal muscle splicing variant of *Mylk4* has a distinct physiological role from both *Mylk2* and the cardiac splicing variant of *Mylk4* and contributes to androgen/AR-induced skeletal muscle strength (Figure S8).

DISCUSSION

In this study, we analyzed androgen function of skeletal muscles mediated by AR. We showed that androgens have two different modes of action on skeletal muscles, a direct pathway and an indirect pathway. DHT treatment increased grip strength in Ctrl mice, whereas DHT treatment failed to increase grip strength in the cARKO mice (Figure 1). Therefore, muscle strength is regulated by AR in skeletal muscles, referred as a direct pathway. In the direct pathway, androgens activate AR in the myofiber to regulate muscle strength. DHT treatment increased skeletal muscle mass both in Ctrl mice and in cARKO mice (Figure 1). Therefore, muscle mass is not regulated by AR in skeletal muscles, referred as an indirect pathway. In the indirect pathway, androgens activate AR in extra-myofiber cells or tissues to regulate muscle mass. RNA-seq analysis revealed direct and indirect target genes of AR, among which we found *Mylk4* as a responsible gene for the regulation of muscle strength. Deletion of *Mylk4* resulted in impaired muscle strength, and phosphoproteomics analysis identified MYOM1 as a substrate of MYLK4. Altogether, our analysis indicated the molecular mechanism of AR-dependent muscle strength through *Mylk4* and MYOM1.

Muscle strength and stiffness

Consistent with previous reports, we also found that androgens directly regulate muscle strength. AR increased the skeletal muscle splicing variant of *Mylk4* gene expression, and *Mylk4* KO mice showed decreased isometric torque. AR-induced muscle strength is, at least in part, achieved by *Mylk4*. In addition, *Mylk4* KO mice had decreased passive stiffness of skeletal muscles. Men's skeletal muscle stiffness is known to be higher than that of women's (Wu et al., 2016). The higher stiffness in men might be due to AR-induced transcriptional regulation of *Mylk4* and phosphorylation of MYOM1 by Mylk4. MYOM1 is known as an important molecule to be a structural linker between the thick filaments and serves as the major cross-linking protein of the M-line and plays a role in organization of sarcomere proteins (Lange et al., 2005; Sweeney and Hammers, 2018). In addition, *in vitro* biochemical analyses revealed that the interaction between myomesin and titin is regulated by the phosphorylation of myomesin (Obermann et al., 1997). Also, *MYOM1* is reported as one of the responsible genes of myotonic dystrophy (Koebis et al., 2011). Thus, MYOM1 and its phosphorylation would have a significant role in regulation of skeletal muscle strength. Still, the physiological significance of phosphorylation of MYOM1 and the relationship between muscle strength and muscle stiffness is not clearly understood, and future study of these topics would be valuable. We would like to note that *Mylk4* is also expressed at low level in the central nervous system, lung, mammary gland, and thymus (Yue et al., 2014); therefore, MYLK4 could phosphorylate an unknown protein in the central nervous system and affect skeletal muscle through a motoneuron or an endocrine system. In addition, we used female mice which have the estrous cycle, so estrogen, progesterone, follicle-stimulating hormone, and luteinizing hormone could also affect the expression of *Mylk4*.

Androgen-induced metabolic change

RNA-seq analysis revealed that muscle AR increased gene expression of glycolysis and decreased gene expression of amino acid catabolism (Figures 2 and S2). This metabolic shift preserves amino acids for protein synthesis. In addition to glycolysis, genes for polyamine metabolism (*Odc1*, *Amd1*, *Smox*) also were induced by myofiber AR in this report, and these genes are well-known targets of AR (Lee and MacLean, 2011). Polyamines decrease with aging, and supplementation with spermidine promoted longevity mediated by induction of autophagy in yeast (Eisenberg et al., 2009). Myopathy in *Col6a1* null mice was ameliorated by spermidine treatment (Chrisam et al., 2015). Spermidine supplementation coupled with exercise ameliorated skeletal muscle atrophy induced by intraperitoneal injection of D-galactose (Fan et al., 2017). These reports suggested that AR-induced polyamine synthesis could increase autophagy flux in skeletal muscles to maintain muscle quality, which might affect consequent muscle strength.

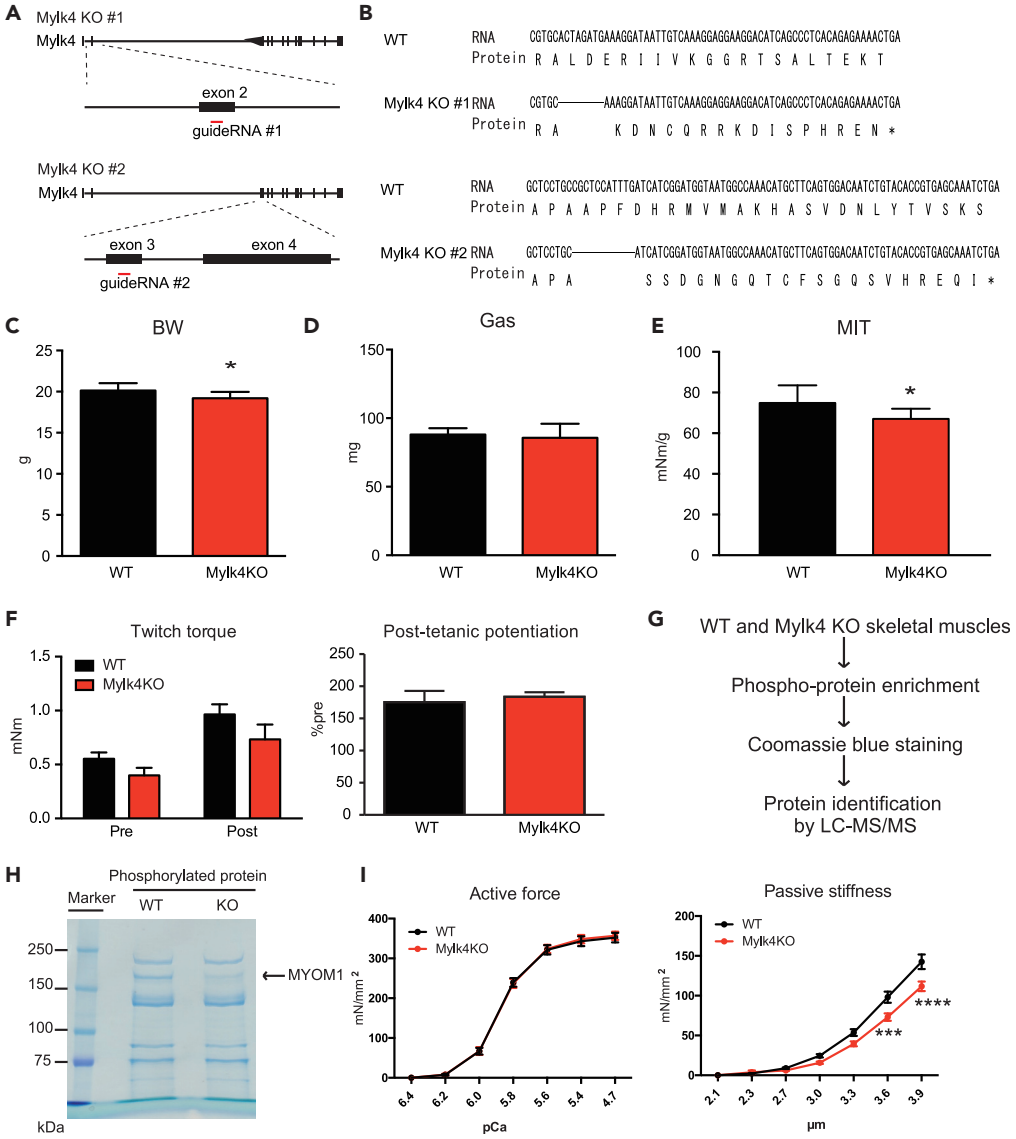

Figure 4. *Mylk4* KO mice showed decreased isometric torque and passive stiffness mediated by phosphorylation of MYOM1

(A) Strategy for generation of Mylk4 KO mice #1 and #2 by the Cas9 system.

(B) Sequence of mRNA and protein of Mylk4 KO mice #1 and #2.

(C–E) Body weight (C), gastrocnemius muscle (Gas) weight (D), and maximum isometric torque (MIT) of *in situ* plantar flexion (E) were measured in 10-week-old female WT (n = 10) and *Mylk4* KO mice (n = 8). *P < 0.05.

(F) Post-tetanic potentiation of *in situ* plantar flexion was measured in 10-week-old female WT (n = 5) and *Mylk4* KO mice (n = 3).

(G) Proteomic strategy for substrate identification.

(H) Phosphorylated proteins were enriched from WT and *Mylk4* KO mice and analyzed by SDS-PAGE.

(I) Active force and passive stiffness were measured with chemically skinned fibers from tibialis anterior muscles of 10-week-old female WT (active force, n = 28; passive force, n = 23) and *Mylk4* KO mice (active force, n = 20; passive force, n = 24). ***P < 0.001, ****P < 0.0001. Two-tailed, unpaired Student's t tests. Data are represented as mean ± standard deviation.

See also Figures S6–S8.

Peroxisome proliferator-activated receptor gamma coactivator 1-alpha (*Ppargc1a*), a key regulator of mitochondrial biogenesis, is induced by synthetic androgen in prostate cancer cells (Tennakoon et al., 2014). However, our RNA-seq analysis did not detected upregulation of *Ppargc1a* in skeletal muscles by DHT treatment. AR would activate its target depending on the context, such as availability of protein complex or epigenetic modification.

The expression of *Mylk4*, *Odc1*, *Amd1*, and *Smox* in soleus muscles, slow-type muscles, was not significantly different between male and female (Figures 3F and S2C). These results suggested that androgen action in slow-type muscles is different from that of fast-type muscles. Further investigation is required to understand androgen action in slow-type muscles.

Indirect pathways

Previous studies focusing on AR and skeletal muscles were mainly conducted on male extragenital muscles such as LA and the bulbocavernosus muscles, which are well known as androgen-sensitive muscles. However, in this study, limb muscle mass was increased by DHT treatment even in cARKO mice (Figure 1). This suggested that increased limb skeletal muscle mass by androgen/AR would be regulated through endocrinological secretion or neuronal pathway by extra-muscle organs expressing *Ar*. Recently, neuron-specific *Ar* knockout mice were reported to have decreased hindlimb muscle mass but muscle strength was not affected (Davey et al., 2017). When testosterone acted on neurons in the dorsal striatum, locomotor activity was increased via dopaminergic pathways (Jardi et al., 2018). These reports indicated muscle mass regulation by a neural circuit. As an effector of muscle mass in skeletal muscles, *Igf1* mRNA expression was decreased in gastrocnemius muscles of neuron-specific AR knockout mice (Davey et al., 2017). In our RNA-seq analysis, *Igf1* was not included in DEGs, but RT-qPCR analysis showed that *Igf1* mRNA was slightly increased by DHT treatment even in cARKO mice (Figure S3). In a C2C12 cell line, testosterone supplementation directly increased *Igf1* mRNA expression (Sculthorpe et al., 2012). So, the regulation of *Igf1* mRNA expression would also be context dependent.

Our RNA-seq analysis revealed that expression levels of 65 genes were increased by DHT treatment even in cARKO mice, which were categorized as DHT-dependent and myofiber AR-independent genes. Among 65 genes, *Ace*, which encodes an angiotensin-1 converting enzyme, showed a clear expression pattern for muscle AR independence and DHT dependence. A human *ACE* gene is known to have a polymorphism characterized by the presence (*ACE-I* allele) or absence (*ACE-D* allele) of a silencer sequence in intron 16 of the *ACE* gene. These polymorphisms of *ACE* allele are correlated with exercise endurance performance (Montgomery et al., 1998; Myerson et al., 1999), suggesting that ACE-angiotensin signaling could regulate skeletal muscle mass. On the other hand, hyperactivity of classical renin-angiotensin system in skeletal muscles is also known to be associated with insulin resistance, atrophy, and fibrosis (Cabello-Verrugio et al., 2015). The physiological role of increased *Ace* expression is still controversial.

In conclusion, this study explored, at least in part, the molecular function underlying the effects of androgen/AR on skeletal muscle, especially for its direct effects (Figure S8). We identified a splicing variant of Mylk4 as a target of AR in skeletal muscle and showed that Mylk4 regulates muscle strength through phosphorylation of MYOM1. Our results will have a significant impact on the understanding muscle strength and contribute to develop a medicine to treat sarcopenia in future. Further studies are needed to fully understand the entire mechanisms of androgen-induced augmentation of skeletal muscle mass and strength.

Limitation of the study

The limitation of our experiment is the small sample size for the quantitative PCR experiment, which might prevent the discovery of AR target genes.

Resource availability

Lead contact

Further information and requests for resources should be directed to and will be fulfilled by the lead contact, M.D., Ph.D. Yuuki Imai, y-imai@m.ehime-u.ac.jp.

Material availability

This study did not generate nor use any new or unique reagents.

Data and code availability

RNA sequencing data have been deposited in the Gene Expression Omnibus as accession no. GSE152756.

METHODS

All methods can be found in the accompanying Transparent Methods supplemental file.

SUPPLEMENTAL INFORMATION

Supplemental information can be found online at https://doi.org/10.1016/j.isci.2021.102303.

ACKNOWLEDGMENTS

The authors thank Dr. Naohito Tokunaga, the staff of the Division of Analytical Bio-Medicine and the Division of Laboratory Animal Research, the Advanced Research Support Center (ADRES), Ehime University. Ms. Aya Tamai and Ms. Sayoko Nakanishi and the members of the Division of Integrative Pathophysiology, Proteo-Science Center (PROS), Ehime University, for their technical assistance and helpful support. We also thank Prof. Ken-Ichiro Morohashi, Prof. Hirotoshi Tanaka, Prof. Yasuyuki Ohkawa, and Dr. Takashi Baba for their helpful discussion. Our study was supported in part by the Japan Society for the Promotion of Science (JSPS) KAKENHI Grants (JP15K16517, JP18K11069, JP17H06427, JP15H04961, JP19H03786), Ehime University PROS, the Osaka Medical Research Foundation for Intractable Diseases, The Nakatomi Foundation (2016ws42), and Takeda Science Foundation.

AUTHOR CONTRIBUTIONS

I.S. and Y.I. conceived and managed the project. Y.Y., K.H., T.Y., and Y.S. generated *Mylk4* KO mice and analyzed the muscle function of *Mylk4* mice. H.S. performed immunostaining of AR. I.S., H.T., A.Y., and T.S. performed proteomics analysis. I.S. and N.S. performed qPCR experiments. H.H. helped the RNA-seq analysis. S.F. advised all aspect of the study. I.S., T.Y., S.F., and Y.I. wrote the manuscript. All the authors discussed and edited the manuscript.

DECLARATION OF INTERESTS

All authors declare no competing interests.

INCLUSION AND DIVERSITY

We worked to ensure diversity in experimental samples through the selection of the cell lines.

Received: November 6, 2020
Revised: February 16, 2021
Accepted: March 10, 2021
Published: April 23, 2021

REFERENCES

Basaria, S., Coviello, A.D., Travison, T.G., Storer, T.W., Farwell, W.R., Jette, A.M., Eder, R., Tennstedt, S., Ulloor, J., Zhang, A., et al. (2010). Adverse events associated with testosterone administration. N. Engl. J. Med. *363*, 109–122.

Bhasin, S., Woodhouse, L., and Storer, T.W. (2001). Proof of the effect of testosterone on skeletal muscle. J. Endocrinol. *170*, 27–38.

Burd, C.J., Morey, L.M., and Knudsen, K.E. (2006). Androgen receptor corepressors and prostate cancer. Endocr. Relat. Cancer *13*, 979–994.

Cabello-Verrugio, C., Morales, M.G., Rivera, J.C., Cabrera, D., and Simon, F. (2015). Renin-angiotensin system: an old player with novel functions in skeletal muscle. Med. Res. Rev. *35*, 437–463.

Chambon, C., Duteil, D., Vignaud, A., Ferry, A., Messaddeq, N., Malivindi, R., Kato, S., Chambon, P., and Metzger, D. (2010). Myocytic androgen receptor controls the strength but not the mass of limb muscles. Proc. Natl. Acad. Sci. U S A *107*, 14327–14332.

Chang, A.N., Mahajan, P., Knapp, S., Barton, H., Sweeney, H.L., Kamm, K.E., and Stull, J.T. (2016). Cardiac myosin light chain is phosphorylated by Ca2+/calmodulin-dependent and -independent kinase activities. Proc. Natl. Acad. Sci. U S A *113*, E3824–E3833.

Chang, C., Yeh, S., Lee, S.O., and Chang, T.M. (2013). Androgen receptor (AR) pathophysiological roles in androgen-related diseases in skin, bone/muscle, metabolic syndrome and neuron/immune systems: lessons learned from mice lacking AR in specific cells. Nucl. Recept. Signal. *11*, e001.

Chrisam, M., Pirozzi, M., Castagnaro, S., Blaauw, B., Polishchuck, R., Cecconi, F., Grumati, P., and Bonaldo, P. (2015). Reactivation of autophagy by spermidine ameliorates the myopathic defects of collagen VI-null mice. Autophagy *11*, 2142–2152.

Davey, R.A., Clarke, M.V., Russell, P.K., Rana, K., Seto, J., Roeszler, K.N., How, J.M.Y., Chia, L.Y., North, K., and Zajac, J.D. (2017). Androgen action via the androgen receptor in neurons within the brain positively regulates muscle mass in male mice. Endocrinology *158*, 3684–3695.

De Gendt, K., and Verhoeven, G. (2012). Tissue- and cell-specific functions of the androgen receptor revealed through conditional knockout models in mice. Mol. Cell. Endocrinol. *352*, 13–25.

Dubois, V., Laurent, M.R., Sinnesael, M., Cielen, N., Helsen, C., Clinckemalie, L., Spans, L., Gayan-Ramirez, G., Deldicque, L., Hespel, P., et al. (2014). A satellite cell-specific knockout of the androgen receptor reveals myostatin as a direct androgen target in skeletal muscle. FASEB J. *28*, 2979–2994.

Eisenberg, T., Knauer, H., Schauer, A., Buttner, S., Ruckenstuhl, C., Carmona-Gutierrez, D., Ring, J., Schroeder, S., Magnes, C., Antonacci, L., et al. (2009). Induction of autophagy by spermidine promotes longevity. Nat. Cell Biol. *11*, 1305–1314.

Fan, J., Yang, X., Li, J., Shu, Z., Dai, J., Liu, X., Li, B., Jia, S., Kou, X., Yang, Y., et al. (2017). Spermidine coupled with exercise rescues skeletal muscle atrophy from D-gal-induced aging rats through enhanced autophagy and reduced apoptosis via AMPK-FOXO3a signal pathway. Oncotarget *8*, 17475–17490.

Ferry, A., Schuh, M., Parlakian, A., Mgrditchian, T., Valnaud, N., Joanne, P., Butler-Browne, G., Agbulut, O., and Metzger, D. (2014). Myofiber androgen receptor promotes maximal mechanical overload-induced muscle hypertrophy and fiber type transition in male mice. Endocrinology *155*, 4739–4748.

Fraysse, B., Vignaud, A., Fane, B., Schuh, M., Butler-Browne, G., Metzger, D., and Ferry, A. (2014). Acute effect of androgens on maximal force-generating capacity and electrically evoked calcium transient in mouse skeletal muscles. Steroids *87*, 6–11.

Jardi, F., Laurent, M.R., Kim, N., Khalil, R., De Bundel, D., Van Eeckhaut, A., Van Helleputte, L., Deboel, L., Dubois, V., Schollaert, D., et al. (2018). Testosterone boosts physical activity in male mice via dopaminergic pathways. Sci. Rep. *8*, 957.

Koebis, M., Ohsawa, N., Kino, Y., Sasagawa, N., Nishino, I., and Ishiura, S. (2011). Alternative splicing of myomesin 1 gene is aberrantly regulated in myotonic dystrophy type 1. Genes Cells *16*, 961–972.

Lange, S., Himmel, M., Auerbach, D., Agarkova, I., Hayess, K., Furst, D.O., Perriard, J.C., and Ehler, E. (2005). Dimerisation of myomesin: implications for the structure of the sarcomeric M-band. J. Mol. Biol. *345*, 289–298.

Lee, N.K., and MacLean, H.E. (2011). Polyamines, androgens, and skeletal muscle hypertrophy. J. Cell. Physiol. *226*, 1453–1460.

MacLean, H.E., Chiu, W.S., Notini, A.J., Axell, A.M., Davey, R.A., McManus, J.F., Ma, C., Plant, D.R., Lynch, G.S., and Zajac, J.D. (2008). Impaired skeletal muscle development and function in male, but not female, genomic androgen receptor knockout mice. FASEB J. *22*, 2676–2689.

Montgomery, H.E., Marshall, R., Hemingway, H., Myerson, S., Clarkson, P., Dollery, C., Hayward, M., Holliman, D.E., Jubb, M., World, M., et al. (1998). Human gene for physical performance. Nature *393*, 221–222.

Myerson, S., Hemingway, H., Budget, R., Martin, J., Humphries, S., and Montgomery, H. (1999). Human angiotensin I-converting enzyme gene and endurance performance. J. Appl. Physiol. *87*, 1313–1316.

Obermann, W.M., Gautel, M., Weber, K., and Furst, D.O. (1997). Molecular structure of the sarcomeric M band: mapping of titin and myosin binding domains in myomesin and the identification of a potential regulatory phosphorylation site in myomesin. EMBO J. *16*, 211–220.

Ophoff, J., Callewaert, F., Venken, K., De Gendt, K., Ohlsson, C., Gayan-Ramirez, G., Decramer, M., Boonen, S., Bouillon, R., Verhoeven, G., et al. (2009). Physical activity in the androgen receptor knockout mouse: evidence for reversal of androgen deficiency on cancellous bone. Biochem. Biophys. Res. Commun. *378*, 139–144.

Rana, K., Chiu, M.W., Russell, P.K., Skinner, J.P., Lee, N.K., Fam, B.C., Zajac, J.D., and MacLean, H.E. (2016). Muscle-specific androgen receptor deletion shows limited actions in myoblasts but not in myofibers in different muscles in vivo. J. Mol. Endocrinol. *57*, 125–138.

Schiaffino, S., and Reggiani, C. (2011). Fiber types in mammalian skeletal muscles. Physiol. Rev. *91*, 1447–1531.

Sculthorpe, N., Solomon, A.M., Sinanan, A.C., Bouloux, P.M., Grace, F., and Lewis, M.P. (2012). Androgens affect myogenesis in vitro and increase local IGF-1 expression. Med. Sci. Sports Exerc. *44*, 610–615.

Stull, J.T., Kamm, K.E., and Vandenboom, R. (2011). Myosin light chain kinase and the role of myosin light chain phosphorylation in skeletal muscle. Arch. Biochem. Biophys. *510*, 120–128.

Sweeney, H.L., and Hammers, D.W. (2018). Muscle contraction. Cold Spring Harb. Perspect. Biol. *10*, a023200.

Tennakoon, J.B., Shi, Y., Han, J.J., Tsouko, E., White, M.A., Burns, A.R., Zhang, A., Xia, X., Ilkayeva, O.R., Xin, L., et al. (2014). Androgens regulate prostate cancer cell growth via an AMPK-PGC-1alpha-mediated metabolic switch. Oncogene *33*, 5251–5261.

Terry, E.E., Zhang, X., Hoffmann, C., Hughes, L.D., Lewis, S.A., Li, J., Wallace, M.J., Riley, L.A., Douglas, C.M., Gutierrez-Monreal, M.A., et al. (2018). Transcriptional profiling reveals extraordinary diversity among skeletal muscle tissues. Elife *7*, e34613.

Wu, R., Delahunt, E., Ditroilo, M., Lowery, M., and De Vito, G. (2016). Effects of age and sex on neuromuscular-mechanical determinants of muscle strength. Age (Dordr) *38*, 57.

Yue, F., Cheng, Y., Breschi, A., Vierstra, J., Wu, W., Ryba, T., Sandstrom, R., Ma, Z., Davis, C., Pope, B.D., et al. (2014). A comparative encyclopedia of DNA elements in the mouse genome. Nature *515*, 355–364.

Zhi, G., Ryder, J.W., Huang, J., Ding, P., Chen, Y., Zhao, Y., Kamm, K.E., and Stull, J.T. (2005). Myosin light chain kinase and myosin phosphorylation effect frequency-dependent potentiation of skeletal muscle contraction. Proc. Natl. Acad. Sci. U S A *102*, 17519–17524.

iScience, Volume *24*

Supplemental information

Myofiber androgen receptor increases muscle strength mediated by a skeletal muscle splicing variant of Mylk4

Iori Sakakibara, Yuta Yanagihara, Koichi Himori, Takashi Yamada, Hiroshi Sakai, Yuichiro Sawada, Hirotaka Takahashi, Noritaka Saeki, Hiroyuki Hirakawa, Atsushi Yokoyama, Soichiro Fukada, Tatsuya Sawasaki, and Yuuki Imai

Figure S1

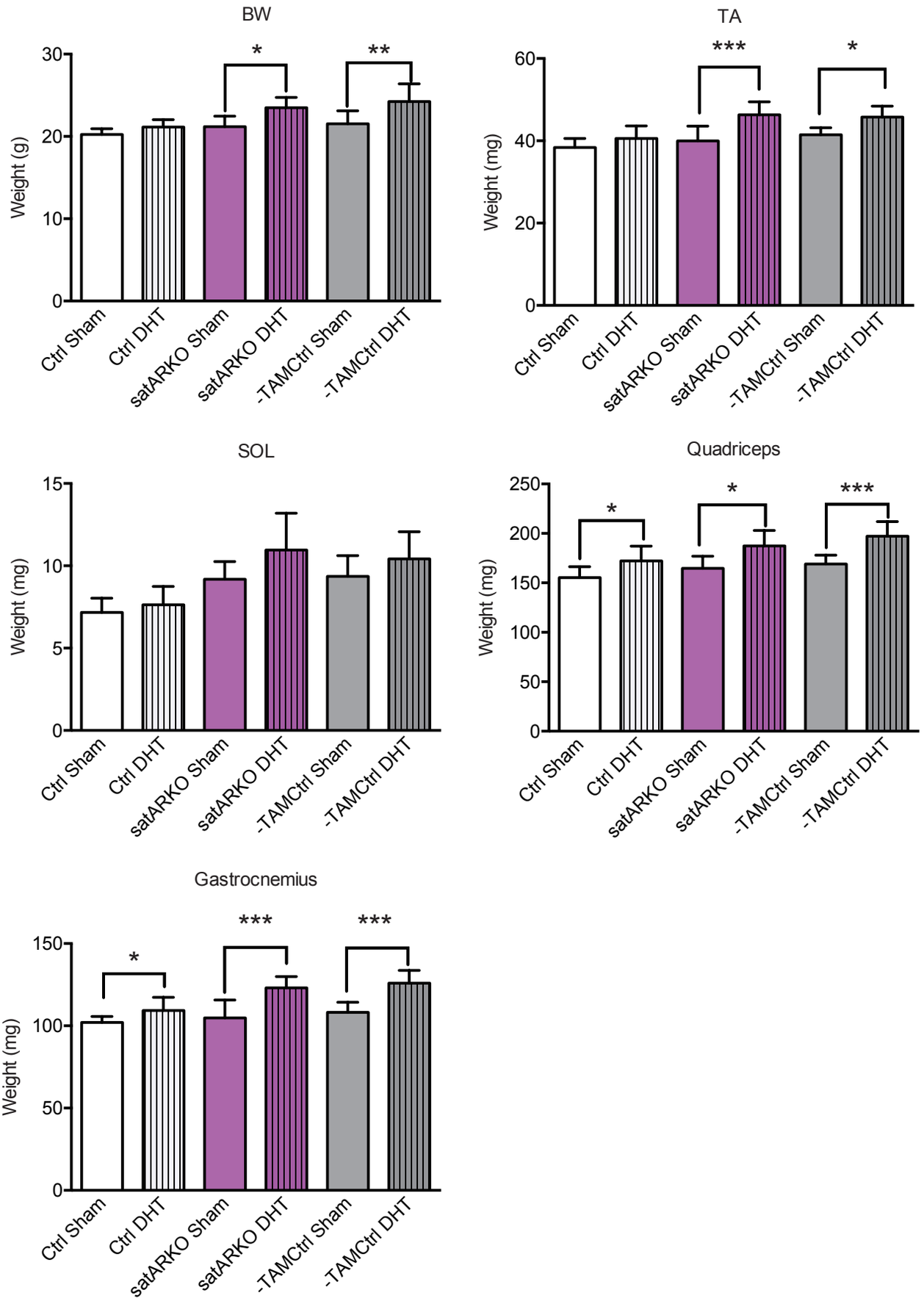
BW
Weight (g)
30
20
10
0
*
**
Ctrl Sham
Ctrl DHT
satARKO Sham
satARKO DHT
-TAMCtrl Sham
-TAMCtrl DHT
TA
Weight (mg)
60
40
20
0
***
*
SOL
Weight (mg)
15
10
5
0
Quadriceps
Weight (mg)
250
200
150
100
50
0
*
*
***
Gastrocnemius
Weight (mg)
150
100
50
0
*
***
***

Figure S2

A

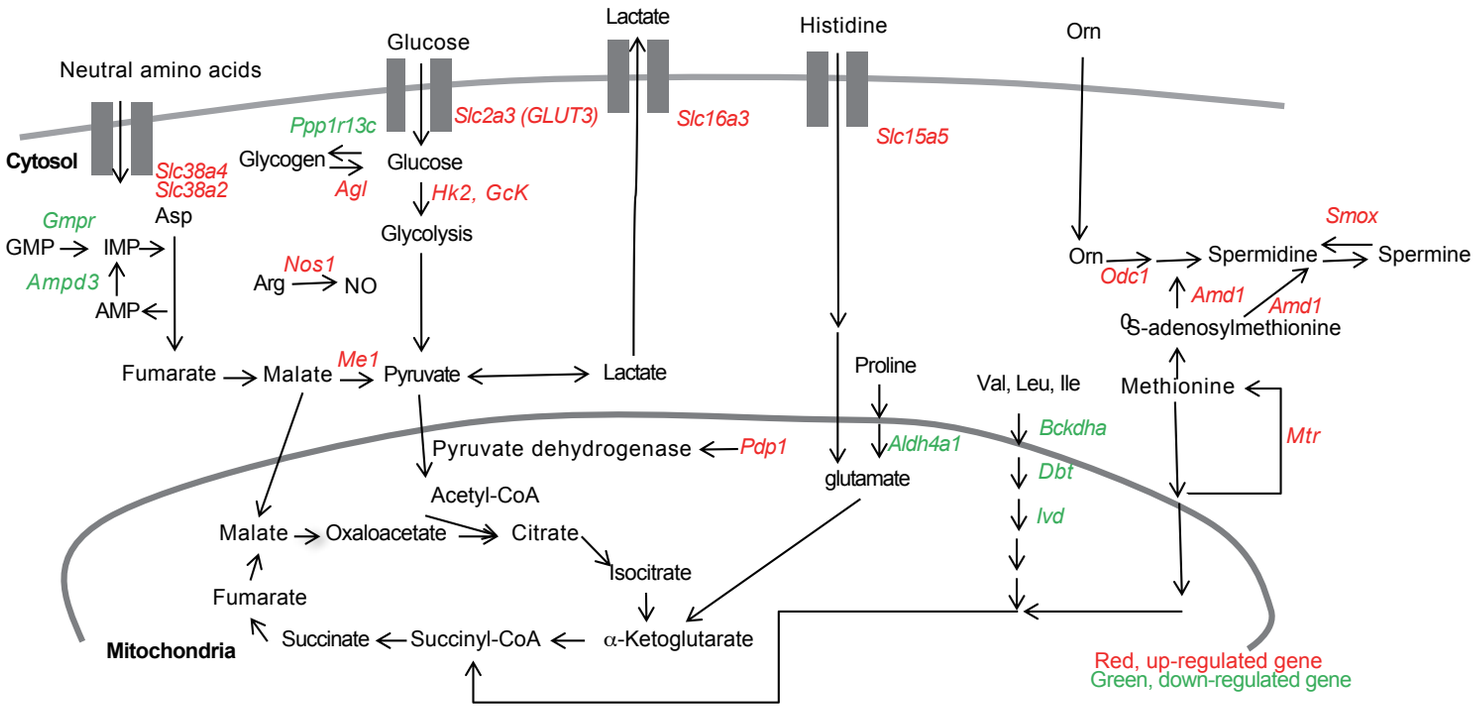

B

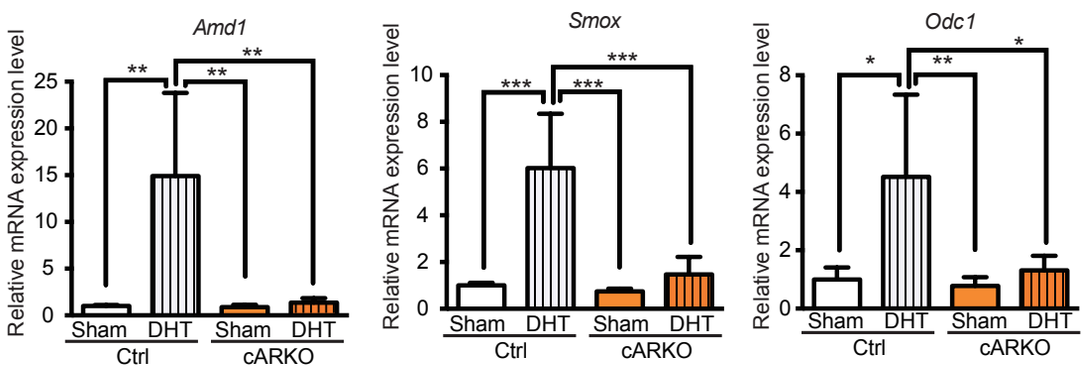

C

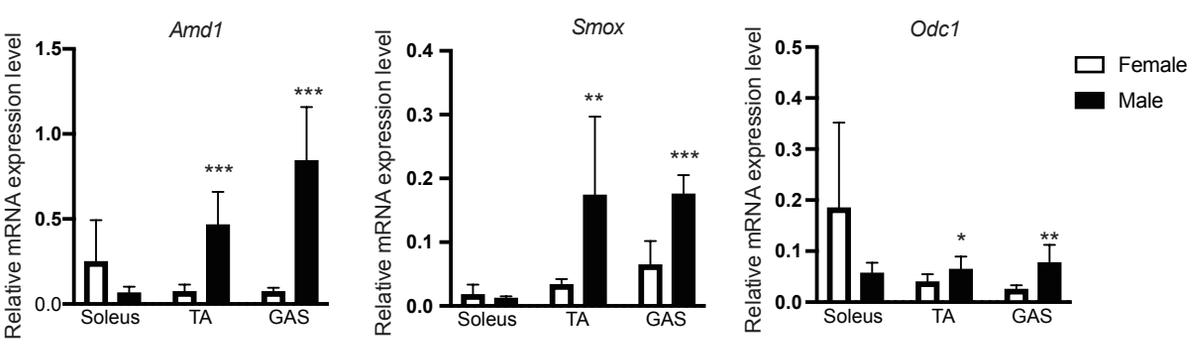

Figure S3

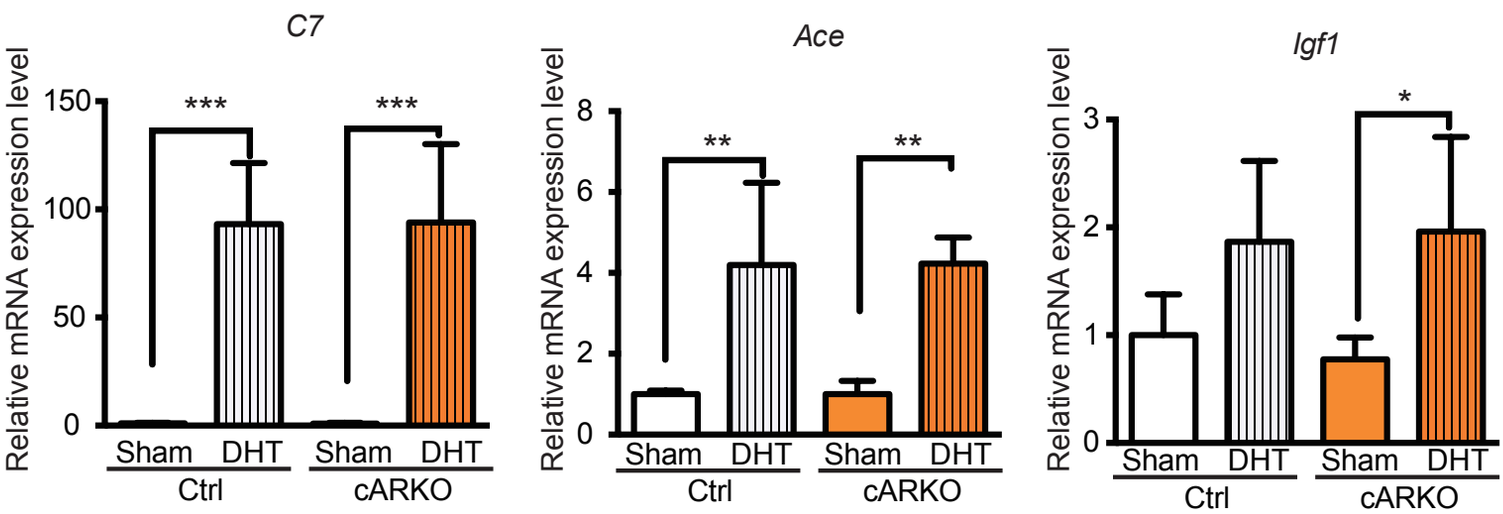
C7
Relative mRNA expression level
150
100
50
0
***
***
Sham
DHT
Sham
DHT
Ctrl
cARKO
Ace
Relative mRNA expression level
8
6
4
2
0
**
**
Sham
DHT
Sham
DHT
Ctrl
cARKO
Igf1
Relative mRNA expression level
3
2
1
0
*
Sham
DHT
Sham
DHT
Ctrl
cARKO

Figure S4

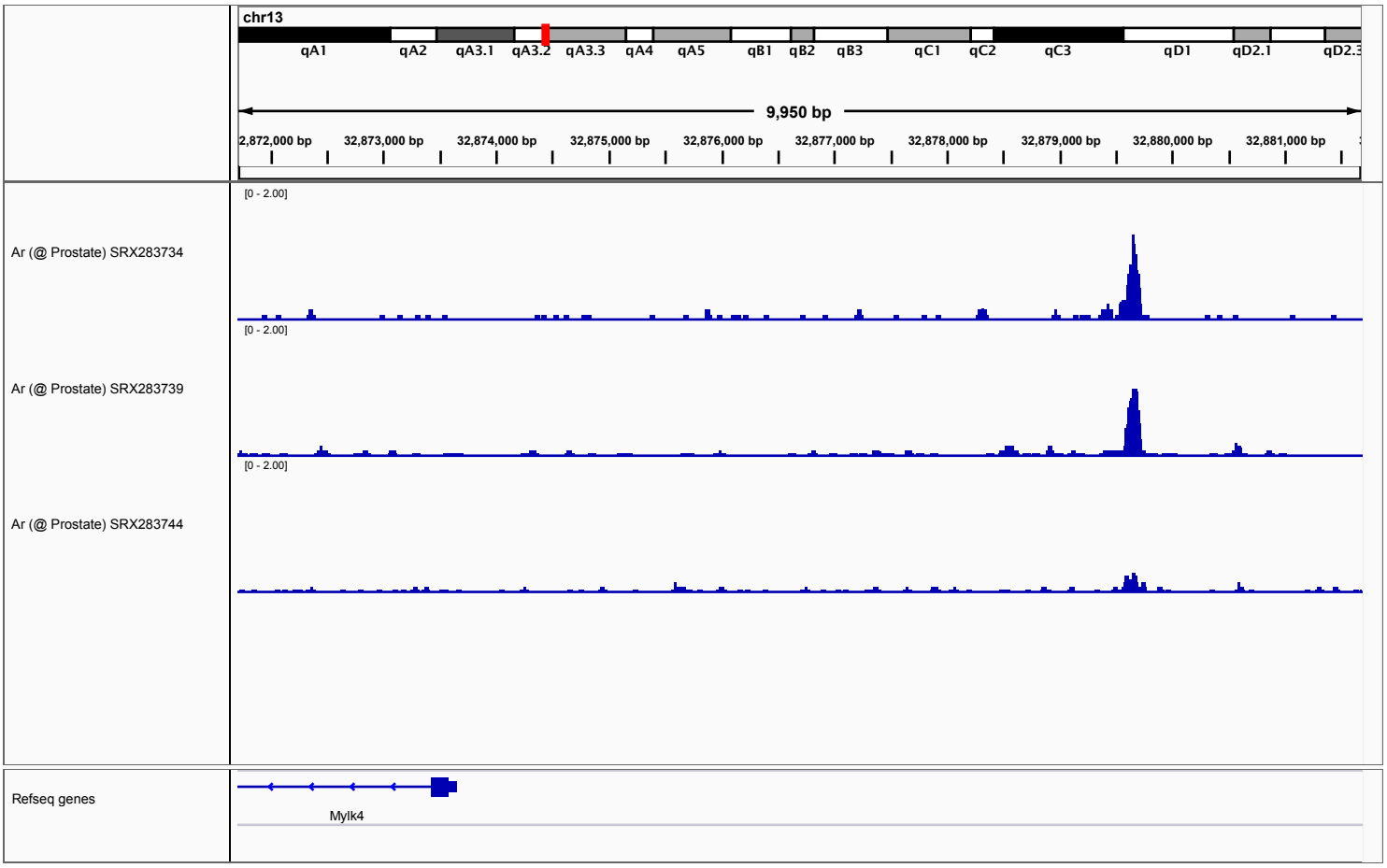
chr13
qA1
qA2
qA3.1
qA3.2
qA3.3
qA4
qA5
qB1
qB2
qB3
qC1
qC2
qC3
qD1
qD2.1
9,950 bp
32,872,000 bp
32,873,000 bp
32,874,000 bp
32,875,000 bp
32,876,000 bp
32,877,000 bp
32,878,000 bp
32,879,000 bp
32,880,000 bp
32,881,000 bp
[0 - 2.00]
Ar (@ Prostate) SRX283734
[0 - 2.00]
Ar (@ Prostate) SRX283739
[0 - 2.00]
Ar (@ Prostate) SRX283744
Refseq genes
Mylk4

Figure S5


MYLK2 ----MTTENGAVELGSQSLSTEQTPKAAAGDGPSASEKEPSAPATEKDLSPPNAKKDPGAPDPKNNPDPPSLKKDPAKAPGPEKKGDPVPASASSQGPSGEGDGGGGPAEGSEGPPAALP
cMYLK4 ----------MLKVKRLEEISSCHSSNPLEKVAFFQCMEEVEKVKCFLEENSGDLDLQSGDNEAEENVWSNRALDERIIVKGGRTSA
skmMYLK4 MSSYRCQEKGVLSSHDCVLIYKSETEGDESPTPDSSLIRLTTSMLKVKRLEEISSCHSSNPLEKVAFFQCMEEVEKVKCFLEENSGDLDLQSGDNEAEENVWSNRALDERIIVKGGRTSA
MYLK2 LPTATAEASIQKLDPTQAPSGNQGSGEAKAG----------KKAAECRE
cMYLK4 LTD----------
skmMYLK4 LTEKTDQNDQFSSEKEKITKLNKKNSEKTSALEVQRSCVICHVERQDKIEFVQRNSTELRENAGAKDAPCIESLEKQESNNLRDKQDTEDNNGGENGISSKDDSRGVEAENRASAAASGA
MYLK2 AGRRGSPAFLHSPSCPAIISCSEKTLAVKPLSETTDLVFTGVSVTPDPQDPGPVKAGGTNALAEKKKEEAEKASGQAGQAKVQGDTPQRIGFQAVPSERVEVGQALCLTAREEDCFQILD
cMYLK4 ----------
skmMYLK4 VLDKHSTESQHTEDMNGDPSHERCISNIKTTSTPGILGNSASGSTFQNAEQTESTGSSKRRVAEECFLSEDNKKSRIDVVRRGEEPTARTEETRQARSLGDRLQDGMTTSREQDLEVPLD
MYLK2 DCPPPPAPFPHRIVELRTGNVNSEFSMNSKEALGGGKFGAVCTCTERATGLKLAAKVIKKQTPKDKEMVLLEIEVMNQLNHRNLIQLYAAIETSHEIILFMEYIEGGELFERIVDEDYHL
cMYLK4 DIPAPAAPFDHRMVMAKHASVDNLYTVSKSEILGGGRFGQVHKCEEKATGLKLAAKIIKTRGAKDKEDVKNEISVMNQLDHVNLIQLYDAFESKHDIILVMEYVEGGELFDRIIDENCNL
skmMYLK4 DIPAPAAPFDHRMVMAKHASVDNLYTVSKSEILGGGRFGQVHKCEEKATGLKLAAKIIKTRGAKDKEDVKNEISVMNQLDHVNLIQLYDAFESKHDIILVMEYVEGGELFDRIIDENCNL
MYLK2 TEVDTMVFVRQICDGILFMHKMRVLHLDLKPENILCVNTTGHLVKIIDFGLARRYNPNEKLKVNFGTPEFLSPEVVNYDQISDKTDMWSLGVITYMLLSGLSPFLGDDDTETLNNVLSAN
cMYLK4 TELDTILFMKQICEGIRYMHQMYILHLDLKPENILCVNRTAKQIKIIDFGLARRYKPREKLKVNFGTPEFLAPEVVNYDFVSFSTDMWSVGVITYMLLSGLSPFLGDNDAETLTNILACR
skmMYLK4 TELDTILFMKQICEGIRYMHQMYILHLDLKPENILCVNRDAKQIKIIDFGLARRYKPREKLKVNFGTPEFLAPEVVNYDFVSFSTDMWSVGVITYMLLSGLSPFLGDNDAETLTNILACR
MYLK2 WYFDEETFEAVSDEAKDFVSNLLTKDQSARMSAEQCLAHPWLNNLAEKAKRCNRRLKSQILLKKYLMKRRWKKNFIAVSAANRFKKISSSGALMALGV
cMYLK4 WDLEDEEFQDISEEAKEFISKLLIKEKSWRISASEALKHPWLSDHKLHSRLSAQKNCNSGVLNLTTK----------
skmMYLK4 WDLEDEEFQDISEEAKEFISKLLIKEKSWRISASEALKHPWLSDHKLHSRLSAQKNCNSGVLNLTTK----------

Figure S6

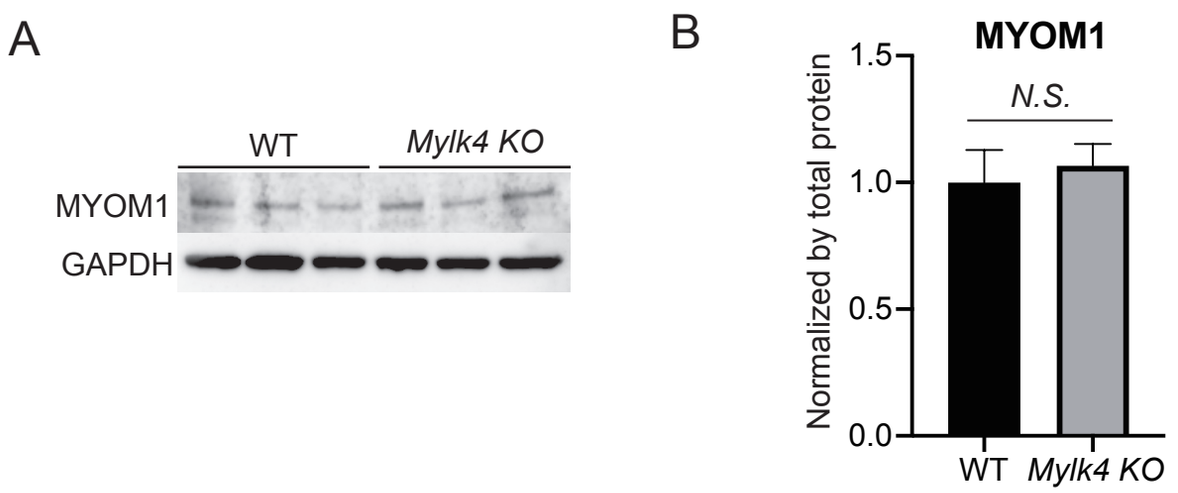
A
WT
Mylk4 KO
MYOM1
GAPDH
B
MYOM1
N.S.
Normalized by total protein
1.5
1.0
0.5
0.0
WT
Mylk4 KO

Figure S7

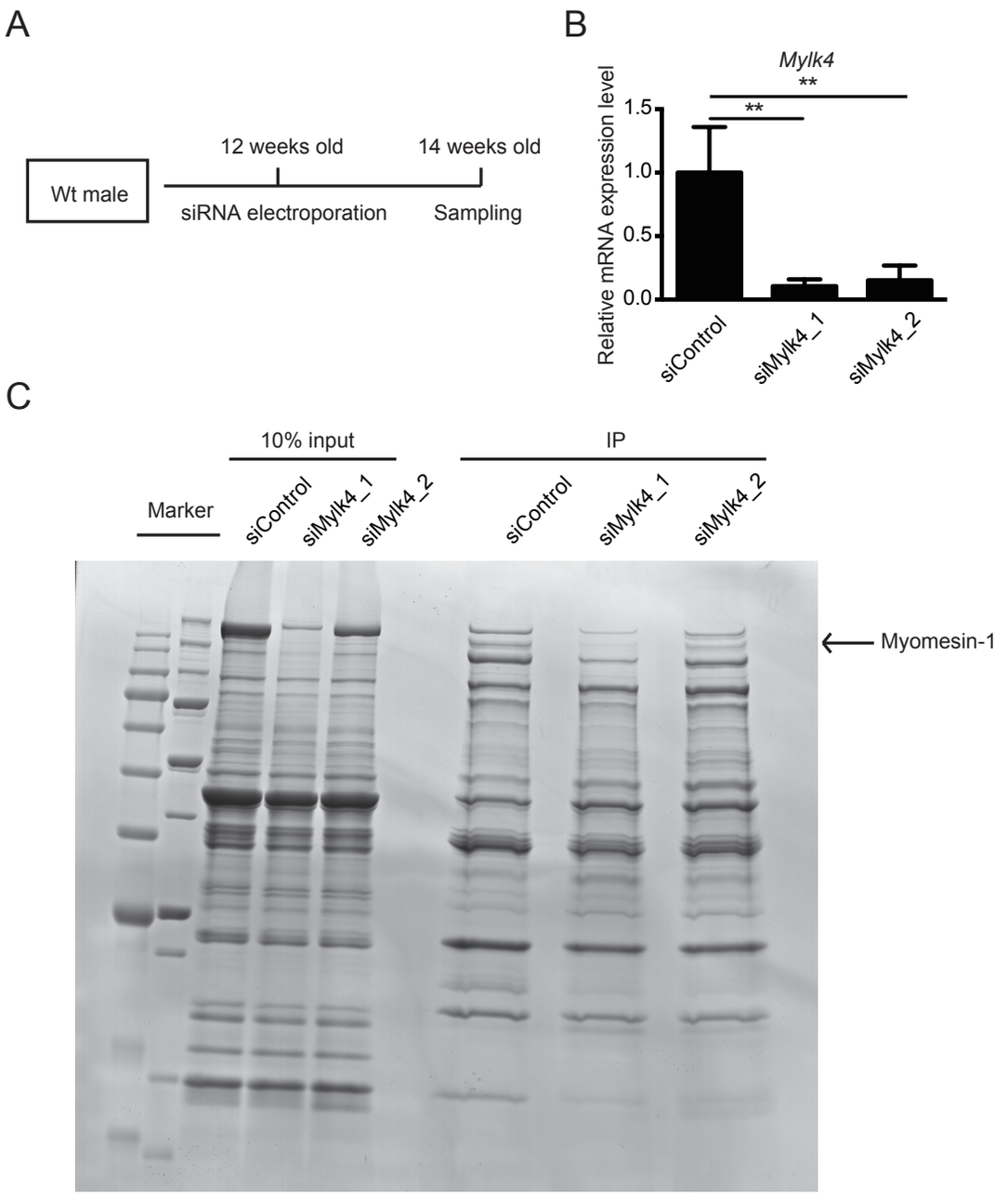
A
12 weeks old
14 weeks old
Wt male
siRNA electroporation
Sampling
B
Mylk4
**
**
Relative mRNA expression level
1.5
1.0
0.5
0.0
siControl
siMylk4_1
siMylk4_2
C
10% input
IP
Marker
siControl
siMylk4_1
siMylk4_2
siControl
siMylk4_1
siMylk4_2
Myomesin-1

Figure S8

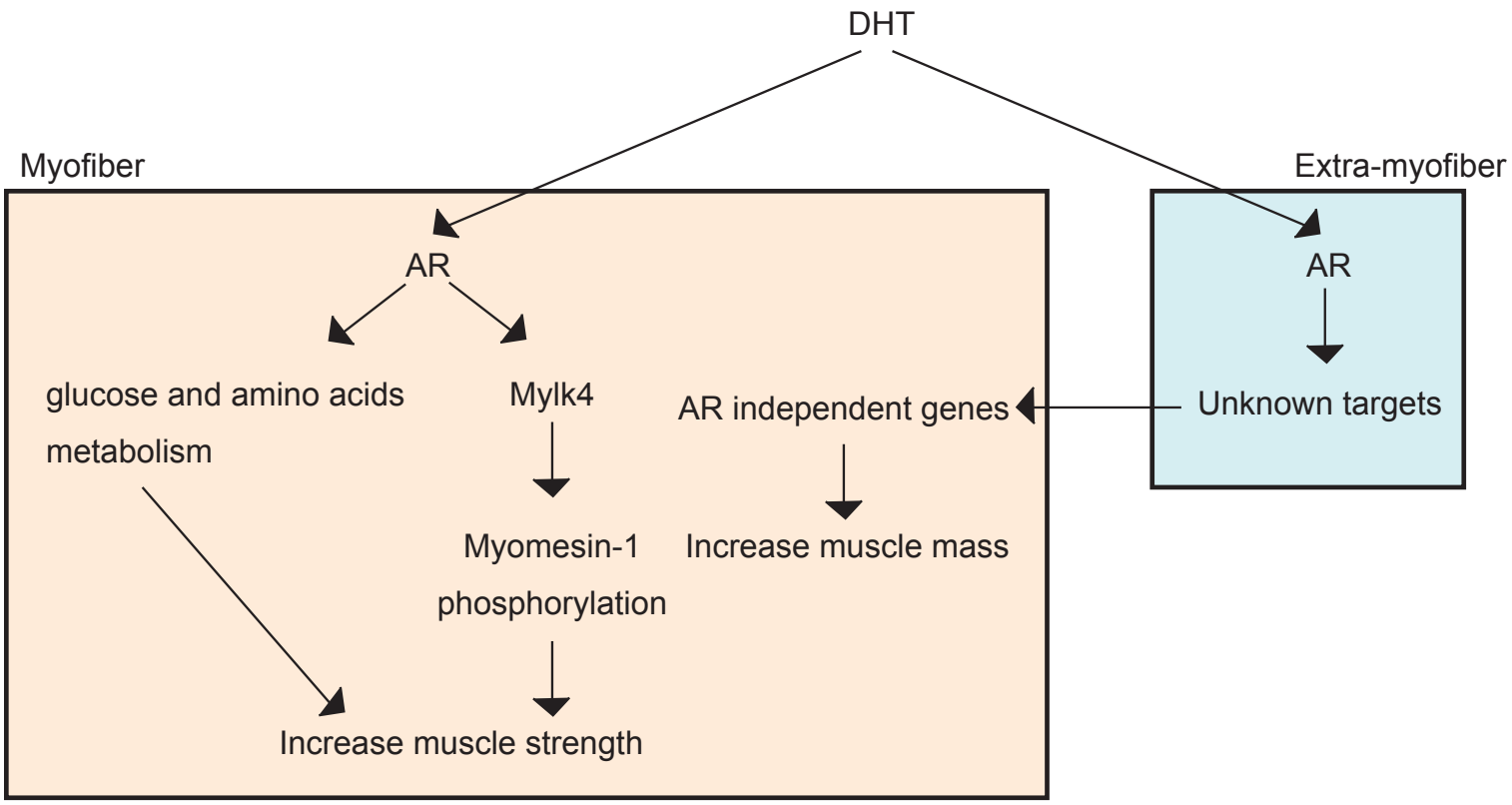
DHT
Myofiber
Extra-myofiber
AR
AR
glucose and amino acids
metabolism
Mylk4
AR independent genes
Unknown targets
Myomesin-1
phosphorylation
Increase muscle mass
Increase muscle strength

Supplemental information

Figure S1. *Ar* deletion in a satellite cell did not affect DHT-induced muscle hypertrophy, Related to Figure 1. Nine-week-old female control and *satARKO* mice were implanted with a pellet containing 10 mg DHT. Body weight, TA muscle weight, soleus muscle (SOL) weight, quadriceps muscle weight, and gastrocnemius muscle weight were measured in 13-week-old female Ctrl_Sham (n=7), Ctrl_DHT (n=6), satARKO_Sham (n=5), satARKO_DHT (n=5), -TAMCtrl_Sham (n=6), and -TAMCtrl_DHT (n=6) mice. Data are represented as mean ± SD. *P<0.05, **P<0.01, ***P<0.001. One-way ANOVA followed by Student Newman-Keuls tests.

Figure S2. Enhanced glucose utilization and suppressed amino acid catabolism by AR, Related to Figure 2. (*A*) Genes coding for the glycolytic pathway and amino acid metabolism are represented. Genes whose expression is modified in *cARKO* are indicated as red (up) or green (down). (*B*) mRNA expression levels of *Amd1*, *Smox and Odc1* in gastrocnemius muscles of 13-week-old female Control_Sham (n=4), Control_DHT (n=3), cARKO_Sham (n=4), and cARKO_DHT (n=5) mice. *P<0.05, **P<0.01, ***P<0.001. (*C*) *Amd1*, *Smox and Odc1* gene expression was determined in soleus muscles, TA muscles, and gastrocnemius muscles of male or female mice by RT-qPCR (n=8, each tissue). Data are represented as mean ± SD. *P<0.05, **P<0.01, ***P<0.001. One-way ANOVA followed by Student Newman-Keuls tests.

Figure S3. mRNA expression levels of *C7*, *Ace and Igf1*, Related to Figure 2. mRNA expression levels of *C7*, *Ace and Igf1* in gastrocnemius muscles of 13-week-old female Control_Sham (n=4), Control_DHT (n=3), cARKO_Sham (n=4), and cARKO_DHT (n=5) mice. Data are represented as mean ± SD. *P<0.05, **P<0.01, ***P<0.001. One-way ANOVA followed by Student Newman-Keuls tests.

Figure S4. AR binding at the *Mylk4* gene locus, Related to Figure 3. Genome viewer for registered ChIP-seq against AR (GSE47119) at the *Mylk4* gene locus in mouse prostates.

Figure S5. Alignment of amino acid sequence of MYLK2, cardiac MYLK4 (cMYLK4) and skeletal muscle MYLK4 (skmMYLK4), Related to Figure 3. '*' indicates positions which have a single, fully conserved residue; ':' indicates that one of the following 'strong' groups is fully conserved: STA, NEQK, NHQK, NDEQ, QHRK, MILV, MILF, HY, FYW; '.' indicates that one of

the following 'weaker' groups is fully conserved: CSA, ATV, SAG, STNK, STPA, SGND, SNDEQK, NDEQHK, NEQHRK, FVLIM, HFY. Amino acid sequence of MYLK2 underlined with red, green and blue indicate kinase domain, autoinhibitory regulatory segment and CaM binding regulatory segment, respectively.

Figure S6. MYOM1 protein levels in Mylk4 KO mice is comparable with WT mice, Related to Figure 4.

(*A*) Western blot analyses for MYOM1 using total lysates of quadriceps muscles obtained from WT and *Mylk4 KO* mice. GAPDH was used as a loading control. (*B*) Quantitative analysis of western blot. The signal of MYOM1 from the immunoblot analyses were normalized to the total protein concentration of each samples and WT signals (n=3). *N.S.* indicates not significant. Two-tailed, unpaired Student's *t* tests.

Figure S7. MYOM1 phosphorylation is decreased by knockdown of *Mylk4*, Related to Figure 4. (*A*) An experimental scheme. TA muscles of 12-week-old male wild type mice were electroporated with 40 pmol siRNA against *Mylk4*. Two weeks later, TA muscles were analyzed. (*B*) *Mylk4* mRNA expression levels in TA muscles of 14-week-old male siControl (n=3), si*Mylk4*_1 (n=3), and si*Mylk4*_2 (n=3) mice. **P<0.01. (*C*) Phosphorylated proteins were enriched from WT and *Mylk4* knockdown mice and analyzed by SDS-PAGE. Two-tailed, unpaired Student's *t* tests. Data are represented as mean ± SD.

Figure S8. A model of AR controlling muscle strength and muscle mass, Related to Figure 4.

TRANSPARENT METHODS

Materials and Methods

Animals and ethics statement

Protocols of animal experiments were approved by the Animal Experiments Committee of Ehime University and Sapporo Medical University, and were performed in accordance with the Guidelines of Animal Experiments of Ehime University and Sapporo Medical University. *Ar*$^{flox/flox}$*;HSA-Cre* conditional knockout mice (*cARKO*) were obtained by breeding *Ar-LoxP* mice (Kato et al., 2004) and transgenic mice expressing a Cre recombinase under the control of the human skeletal actin promoter (HSA) (Miniou et al., 1999). *Ar*$^{flox/flox}$*;Pax7*$^{CreERT2/+}$ conditional

knockout mice (*satARKO*) were obtained by breeding *Ar-LoxP* mice (Kato et al., 2004) and knock-in mice expressing a Cre^{ERT2} recombinase under the control of the *Pax7* promoter (Lepper et al., 2009). Eight-week-old female *satARKO* mice were given intraperitoneal injection of tamoxifen (1 mg per mouse per day; Sigma) for 5 consecutive days. DHT tablet (SA-161, Innovative Research of America, Sarasota, FL, USA) implantation was performed under isoflurane anesthesia, and all efforts were made to minimize suffering. Each littermate group was divided into the Sham operation group or DHT supplementation group, equally as possible.

Grip strength

Mice forelimb grip strength was measured with a strain gauge (GPM-100B, Melquest, Toyama City, Toyama, Japan). Measurements were repeated ten times, and the maximal force was recorded. The mean value of two records was used as the grip strength of each mouse.

RNA preparation

Gastrocnemius muscles were collected from *cARKO* and control mice. Total RNAs were extracted using ISOGEN Reagent (Nippon Gene, Chiyoda, Tokyo, Japan) and RNeasy Mini Kit (Qiagen, Hilden, Germany) according to the manufacturer's instructions.

cDNA synthesis and qPCR

RNAs were reverse-transcribed with PrimeScript RT Master Mix (RR036A, Takara, Kusatsu, Shiga, Japan) according to the manufacturer's instructions. Reverse transcription was performed with 500 ng of total RNA. Quantitative real time PCR was performed using SYBR Premix Ex Taq II (RR820L, Takara, Kusatsu, Shiga, Japan) according to the manufacturer's protocols. PCR was performed for 40 cycles at 95 °C for 5 seconds and 60 °C for 30 seconds using the Thermal Cycler Dice Real Time System (Takara, Kusatsu, Shiga, Japan). Gene expression levels were normalized by the expression level of the housekeeping gene *Actb*. The sequences of the oligonucleotides used in this study are given in Supplementary Table S1. For PCR analysis of Mylk4, fragments were amplified with forward 5'-GAGATGAAAGCCCCACTCCT -3' and reverse 5'- CTCCAATGCATCCTCCAGAT -3'.

RNA sequencing

Libraries were generated from one μg of total RNA by a TruSeq Stranded mRNA LT Sample Prep Kit (Illumina, San Diego, CA, USA) according to the manufacturer's instructions. 18 pM of

each library was sequenced on Miseq (Illumina) with MiSeq Reagent kit V3 150 cycle (Illumina, San Diego, CA, USA) by 75 base pair end. The reads were mapped on the mouse genome (mm10) by Tophat, and read numbers were counted by FeatureCounts. Differentially expressed genes were determined by an exact test after normalization. RNA sequencing data have been deposited in the Gene Expression Omnibus as accession no. GSE152756. Hierarchical clustering of 529 DEGs was performed by MeV software (Saeed et al., 2003). Pathway analysis was performed by using DAVID Bioinformatics Resources(Huang da et al., 2009a, b).

Immunoblot Analysis

Homogenized tissues were lysed in RIPA buffer (10 mM Tris HCL (pH 7.4); 150 mM NaCl, 5 mM EDTA (pH 7.4); 1% Triton X-100; 1% Sodium deoxycholate; 0.1% sodium dodecyl sulphate) supplemented with protease inhibitor cocktail (Nacalai Tesque, Kyoto, Japan). The immunoblot analysis was performed with tissue lysates of quadriceps muscles using the capillary electrophoresis system (Jess, ProteinSimple). Samples were loaded on the Jess separation module (12 to 230 kDa). The Myomesin 1 peaks were normalized to the total protein concentration using a protein normalization kit (ProteinSimple) and quantified using the Jess quantification module.

Immunohistochemistry

Immunofluorescence staining for AR was performed as previously described (Sakai et al., 2020) with modifications. Briefly, muscles were frozen in liquid nitrogen-chilled isopentane. For immunofluorescence staining, 10 μm cryosections were collected and sections were fixed with 4% paraformaldehyde (PFA) in PBS for 5 min followed by permeabilization with a buffer containing 0.3% Triton X-100 in PBS for 10 min. Slides were washed, blocked with 5% goat serum in PBS and incubated with respective antibodies overnight at 4˚C. The slides were washed and stained with secondary antibodies. Antibodies used for the immunofluorescence were anti-AR (Abcam, Cat# ab105225) and Alexa fluor 488 goat anti-rabbit IgG (Invitrogen, Cat# A-11008).

Electroporation

In vivo transfections were carried out on 12-week-old C57Bl6N mice. For each experimental condition, three to five TA muscles belonging to different mice were used. Under isoflurane anesthesia, legs were shaved and muscles were pre-treated by injection of a sterile 0.9% NaCl

solution containing 0.4U of bovine hyaluronidase/μl two hours before siRNA injection. Four hundred pmol of stealth siRNA (Invitrogen, Carlsbad, CA, USA) and 100 ng of GFP expression plasmid were introduced into TA muscles by electroporation as previously described (Sakakibara et al., 2016). Two weeks following electroporation, mice were euthanized and electroporated muscles were frozen in liquid nitrogen before processing for RNA or protein extraction.

Phosphoprotein proteomics

Phosphoproteins were enriched from TA muscle lysates by a TALON PMAC Magnetic phosphoprotein enrichment kit (635641, Clontech) according to the manufacturer's instructions. The eluate fractions were analyzed by SDS-PAGE, and bands were excised from the gel and analyzed by LC-MS/MS. Briefly, extracted peptides were analyzed by ESI-MS/MS using a Q Exactive Orbitrap instrument (Thermo Fisher Scientific, Pittsburgh, PA, USA). MS spectra were recorded over a range of 350−1500 m/z, followed by data-dependent higher energy collisional dissociation (HCD) MS/MS spectra generated from the ten highest intensity precursor ions. For protein identification, spectra were processed using Proteome Discoverer Version 1.3.0.339 (Thermo Fisher Scientific) against the Mascot algorithm. For database searches, mouse.fasta built from the SwissProt was used. The following parameters were used for the searches: tryptic cleavage, up to two missed cleavage sites, and tolerances of ± 10 ppm for precursor ions, and ± 0.5 Da for MS/MS fragment ions. Mascot searches were performed allowing optional methionine oxidation, serine/threonine phosphorylation and fixed cysteine carbamidomethylation. Proteins that contained peptides with Mascot Significance Threshold > 0.05 were selected.

Generation of *Mylk4* knockout mice

Mylk4 knockout mice were generated by CRISPR/ Cas9-based genome editing delivered by electroporation as previously described (Hashimoto and Takemoto, 2015). The guide RNA sequences were 5'-TTCATCTAGTGCACGGTTGG-3' and 5'-CATCCGATGATCAAATGGAG-3'.

Measurement of *in situ* maximum isometric torque and post-tetanic potentiation

Measurement of *in situ* maximum isometric torque (MIT) and post-tetanic potentiation was described previously (Bowslaugh et al., 2016; Yamada et al., 2019). In short, plantar flexor (PF)

muscles were stimulated supra-maximally (45V, 0.5 ms monophasic rectangular pulse) using a pair of surface electrodes that were placed on the skin. Isometric twitch responses in PF muscles were obtained one min before and 15 s after a potentiating stimulus (PS) consisting of four brief trains of 150 Hz stimulation of 400 ms duration (i.e., MIT) within 10 s (Bowslaugh et al., 2016). Immediately after the measurement, mice were euthanized by cervical dislocation under isoflurane anesthesia and the PF muscles were excised from each animal. Absolute PF torque was normalized to the whole muscle weight for PFs. Post-tetanic potentiation was calculated as the post-PS value divided by the pre-PS value.

Measurement of active and passive force in skinned fibers

The preparation of chemically skinned fiber and the measurement of Ca^{2+}-activated force were described previously (Yamada et al., 2019). A part of the excised TA muscle was pinned out at resting length under paraffin oil and was kept at 4°C. The single muscle fibers were dissected under a stereo-microscope. Four to six skinned fibers were obtained from one whole muscle. A segment of the skinned fiber was connected to a force transducer (Muscle tester, World Precision Instruments) and then incubated with a *N*-2-hydroxyethylpiperazine-*N*'-2-ethanesulfonic acid (HEPES) buffered solution (see below) containing the detergent Triton X-100 (1% (v/v), 10 min treatment) to remove all membranous structures. Fiber length was adjusted to optimal length (2.5 μm) by laser diffraction as described previously (Allen and Kurihara, 1982) and the contractile properties were measured at room temperature (24°C). The solutions used in the skinned fiber analyses were composed of 36 mM Na^+, 126 mM K^+, 90 mM HEPES, 8 mM ATP and 10 mM creatine phosphate, and had a pH of 7.09–7.11 at 24°C (Watanabe and Wada, 2016). The free Mg^{2+} concentration was set at 1.0 mM. The maximum Ca^{2+} solution additionally contained 49.5 mM Ca-EGTA and 0.5 mM free EGTA whereas the relaxation solution contained 50 mM free EGTA. Force-pCa (-log free Ca^{2+} concentration) curves were established with various pCa solutions (pCa 6.4, 6.2, 6.0, 5.8, 5.6, 5.4, and 4.7) prepared by mixing the maximum Ca^{2+} solution and the relaxation solution in appropriate ratios according to the affinity constants reported by Moisescu and Thieleczek (Moisescu and Thieleczek, 1978). The contractile apparatus was directly activated by exposing the skinned fiber to various pCa solutions and the peak force production in each pCa was measured.

The activating solution was then replaced with relaxing solution and the passive force was measured as described previously (Prado et al., 2005). Fibers were stretched from slack sarcomere length (SL, 2.0-2.2 μm) in six steps of ~0.2 μm/sarcomere (complete within 1 s) to a maximum SL, while passive force was recorded during a 2 min pause after each step. Following the last stretch-hold, fibers were released back to slack SL to test for possible shifts of baseline force. From the recordings, we measured the force at the end of each hold period. The cross-sectional area of fibers was calculated from measurements of their diameters. All skinned fibers were used to determine the Ca^{2+}-activated and passive force per cross-sectional area.

Determination of serum DHT

Serum DHT levels were determined by ELISA with a dihydrotestosterone ELISA kit (KA1886, Abnova) according to the manufacturer's instructions.

Statistical analyses

All graphs represent mean values ± SD. Significant differences between mean values were evaluated using two-tailed, unpaired Student's *t* tests (when two groups were analyzed) or one-way ANOVA followed by Student Newman-Keuls tests (for three or more groups).

Supplemental References

Allen, D.G., and Kurihara, S. (1982). The effects of muscle length on intracellular calcium transients in mammalian cardiac muscle. J Physiol *327*, 79-94.

Bowslaugh, J., Gittings, W., and Vandenboom, R. (2016). Myosin light chain phosphorylation is required for peak power output of mouse fast skeletal muscle in vitro. Pflugers Archiv : European journal of physiology *468*, 2007-2016.

Hashimoto, M., and Takemoto, T. (2015). Electroporation enables the efficient mRNA delivery into the mouse zygotes and facilitates CRISPR/Cas9-based genome editing. Sci Rep *5*, 11315.

Huang da, W., Sherman, B.T., and Lempicki, R.A. (2009a). Bioinformatics enrichment tools: paths toward the comprehensive functional analysis of large gene lists. Nucleic acids research *37*, 1-13.

Huang da, W., Sherman, B.T., and Lempicki, R.A. (2009b). Systematic and integrative analysis of large gene lists using DAVID bioinformatics resources. Nat Protoc *4*, 44-57.

Kato, S., Matsumoto, T., Kawano, H., Sato, T., and Takeyama, K. (2004). Function of androgen receptor in gene regulations. The Journal of steroid biochemistry and molecular biology *89-90*, 627-633.

Lepper, C., Conway, S.J., and Fan, C.M. (2009). Adult satellite cells and embryonic muscle progenitors have distinct genetic requirements. Nature *460*, 627-631.

Miniou, P., Tiziano, D., Frugier, T., Roblot, N., Le Meur, M., and Melki, J. (1999). Gene targeting restricted to mouse striated muscle lineage. Nucleic acids research *27*, e27.

Moisescu, D.G., and Thieleczek, R. (1978). Calcium and strontium concentration changes within skinned muscle preparations following a change in the external bathing solution. J Physiol *275*, 241-262.

Prado, L.G., Makarenko, I., Andresen, C., Kruger, M., Opitz, C.A., and Linke, W.A. (2005). Isoform diversity of giant proteins in relation to passive and active contractile properties of rabbit skeletal muscles. J Gen Physiol *126*, 461-480.

Saeed, A.I., Sharov, V., White, J., Li, J., Liang, W., Bhagabati, N., Braisted, J., Klapa, M., Currier, T., Thiagarajan, M.*, et al.* (2003). TM4: a free, open-source system for microarray data management and analysis. Biotechniques *34*, 374-378.

Sakai, H., Sato, T., Kanagawa, M., Fukada, S., and Imai, Y. (2020). Androgen receptor in satellite cells is not essential for muscle regenerations. Experimental Results *1*, e21.

Sakakibara, I., Wurmser, M., Dos Santos, M., Santolini, M., Ducommun, S., Davaze, R., Guernec, A., Sakamoto, K., and Maire, P. (2016). Six1 homeoprotein drives myofiber type IIA specialization in soleus muscle. Skeletal muscle *6*, 30.

Watanabe, D., and Wada, M. (2016). Predominant cause of prolonged low-frequency force depression changes during recovery after in situ fatiguing stimulation of rat fast-twitch muscle. Am J Physiol Regul Integr Comp Physiol *311*, R919-R929.

Yamada, T., Ashida, Y., Tatebayashi, D., and Himori, K. (2019). Myofibrillar function differs markedly between denervated and dexamethasone-treated rat skeletal muscles: Role of mechanical load. PLoS One *14*, e0223551.